



Eidgenössische Technische Hochschule Zürich
Swiss Federal Institute of Technology Zurich

PAUL SCHERRER INSTITUT



s-BASED MAPS FROM TPS & LIE-SERIES APPLIED TO PROTON-THERAPY GANTRIES

MASTER THESIS

in Biomedical Engineering - Medical Physics

Department of Information Technology and Electrical Engineering

ETH Zurich

written by

BSc TU VIENNA
PHILIPPE GANZ

supervised by

Prof. Dr. A. J. Lomax
Dr. A. Adelmann

June 01, 2017

Abstract

Proton therapy is a growing field in radio oncology. It gains its popularity due to the characteristic energy deposition in the tissue, the Bethe-Bloch-Law, resulting in the Bragg-Peak. This allows a decrease the unwanted integral dose and also the sparing of the surrounding healthy tissue. To make full usage of this profitable property gantries are used to provide a beam delivery in different angles. These gantries often contain a quite complex beam optics to ensure a clearly defined beam, as the last beam line section before the patient.

Their design can be done in several beam optics programs, which contain different mathematical approaches. One of those is map tracking. In this method each beam line element gets represented in a multidimensional transfer map. This mathematical description not only simplifies the handling, but also allows a sophisticated beam line analysis. Furthermore, these maps can be combined, to summarize sections in one map and to accelerate the simulation in repetitive sections.

This thesis is based on the idea to implement an map tracking based algorithm in the OPAL framework [1] based on Lie Algebra and Truncated Power Series [2]. Furthermore it was tested it on the therapeutic proton therapy gantry "PSI Gantry 2".

Contents

1	Introduction	1
1.1	Motivation	1
1.2	Theoretical Introduction	1
1.2.1	Beam Optics Formalism	2
1.2.2	Basic Idea of Map Tracking	4
1.2.3	Hamiltonian Mechanic	5
1.2.4	Creation of Hamiltonians	6
1.2.5	Truncated Power Series Algebra	9
1.2.6	Map Creation - Lie Algebra	11
1.2.7	Map Analysis	12
2	Implementations	15
2.1	OPAL-map	15
2.1.1	Introduction	15
2.1.2	Flow Chart	15
2.1.3	DA Package	16
2.1.4	Map Analysis	16
2.2	COSY Infinity	16
2.3	pyAcceLEGOrator	17
3	Results	18
3.1	FODO Cell	18
3.2	FODO + Dipole	23
3.3	Synchrotron	26
3.4	PSI Gantry 2	27
4	Discussion	34
4.1	Map Comparison	34
4.1.1	Map precision	34
4.2	Envelopes	35
4.2.1	Pole Face Rotation	35
4.3	Dispersion	37
4.4	Complexity	38
4.4.1	Accumulation of element maps	38
4.4.2	Tracking through maps	39
5	Conclusion	40
5.1	Outlook	41

6 Acknowledgement	42
7 Acronyms	43
A Units	44
B complete transfer matrix FODO	45
C Canonical Transformations	48
C.1 Canonical transformation of the independent variable $t \rightarrow s$	48
C.2 Canonical transformation of the dependent variable $E \rightarrow \delta$	49
C.3 Canonical transformation for curved trajectories	50
D Complete Transfer Map PSI Gantry 2	52

List of Figures

1.1	Frenet-Serret Coordinates	3
1.2	Pole Face Rotation	8
1.3	Graphical representation of Differential Algebra (DA) and its operators.	10
1.4	Number of monomials in $_nD_6$	11
2.1	OPAL-map flow chart	16
3.1	”FODO” envelopes plot (1 st Order)	19
3.2	FODO with divergent beam and $\delta = 0$	20
3.3	FODO with divergent beam and $\delta \neq 0$	21
3.4	The transfer map of the FODO for the x coordinate up to the third order	22
3.5	”FODO” map comparison	23
3.6	”FODO + Dipole” envelopes plot (1 st Order)	24
3.7	”FODO + Dipole” map comparison	25
3.8	”FODO + Dipole” dispersion plot	26
3.9	Synchrotron envelopes of in 1 st order	26
3.10	Synchrotron dispersion plot	27
3.11	Gantry 2 Elements	28
3.12	PSI gantry 2 envelopes in 1 st order (no dipole pole face rotation)	29
3.13	PSI gantry 2 map comparison	29
3.14	PSI gantry 2 Dispersion plot	30
3.15	PSI gantry 2 envelope plot in the first three orders	31
3.16	PSI gantry 2 difference in envelope plot in the first three orders	31
3.17	The transfer map of the PSI Gantry 2 for the x coordinate up to the second order	32
3.18	PSI gantry 2 simulation timing	32
3.19	PSI gantry 2 envelopes including pole face rotation in 1 st order	33
4.1	PSI gantry 2 envelope comparison in y-plane in- and excluding pole face rotation (PFR)	35
4.2	PSI gantry 2 magnetic fields in y-axis	36
4.3	PSI Gantry 2 envelopes field map comparison	37
4.4	Number of multiplications in $_nD_6$ in order n	39

List of Tables

2.1	The difference in constants of COSY Infinity and OPAL-map	16
3.1	Quadrupole settings of FODO cell	18
3.2	Synchrotron electron beam settings	23
3.3	Settings taken from Synchrotron example	23
3.4	Initial Dispersion taken from Synchrotron example	25
3.5	Beta tunes of Synchrotron	27
3.6	PSI Gantry 2 proton beam settings	28
A.1	Units	44

Chapter 1

Introduction

1.1 Motivation

In 2015 cancer was the cause of death in nearly 8.8 million cases, which makes it to the leading cause of death worldwide. [3, Chapter 1.1] An established non invasive method for its treatment is radiation therapy. Just three months after the discovery of x-rays of Wilhelm Röntgen (1845 - 1923) in 1895 the first treatments took place. Approximately half a century later, in 1946, the accelerator technology has evolved on a level that Robert R. Wilson (1914 - 2000) proposed the use protons (and heavy ions) for the dose delivery [4, Chapter 1.1].

The depth dose distribution of a proton beam is described in the Bethe-Bloch-Law and forms the Bragg-Peak. This property opens new possibilities for treating tumors for example in the eye, brain or spine, due to its finite range. It also can lead to an optimized treatment in which the surrounding healthy tissue receives less dose, resulting in a lower integral dose, which reduces the risk of secondary tumors. This issue is of great importance in a treatment of pediatric patients.

In complex treatment cases it is necessary to deliver multiple fields at different angles to gain an adequate dose distribution, avoiding the radiation of organs at risk. Gantry provide this wanted characteristics.

In an beam optical view, the design of those can be challenging, considering the beam dispersion or beam scanning. For the calculation, different approaches are possible. In this thesis we will focus Map Tracking (MT), in particular on the map creation in Lie-Algebra and the implementation using Truncated Power Series Algebra (TPSA). In this method a mathematical object in form of a (non-) linear "map" gets created for each element. This does not only provide a handy mathematical description of the beam line, but also opens the possibility for beam line analysis or computational speedups.

1.2 Theoretical Introduction

The theoretical introduction is widely adopted from M. Berz [2], F. Hinterberger [5], A. Adelmann [6] and M. Bartelmann [7].

1.2.1 Beam Optics Formalism

Particle

In beam optics the particle gets described by its kinetic attributes, hence the rest mass, charge and the kinematic characteristics. Since the kinematics were defined by the initial position and the movement, a three dimensional system is described by six variables, represented in the six dimensional phase space. In this thesis these six variables refer to a in particle physics widely used convention.

$$\vec{v} = \begin{pmatrix} x \\ p_x \\ y \\ p_y \\ z \\ \delta \end{pmatrix} \quad (1.1)$$

$$\delta = \frac{E}{P_0 c} - \frac{1}{\beta_0} \quad (1.2)$$

$$p_i = \frac{1}{P_0} m u_i = \frac{1}{P_0} \gamma m_0 \frac{\partial i}{\partial t} \quad i = x, y, z \quad (1.3)$$

In the upper formulas E represents the total energy of the particle and P_0 the momentum of the reference particle. β is the relativistic quantity $\beta = \frac{|\vec{u}|}{c}$, defined by the ratio of the absolute particle velocity \vec{u} to the speed of light c .

Using a Frenet-Serret Coordinates (FSC) referring to a Reference Particle (RP) which has the ideal design properties, the variables x , y and z display the spatial offset to the RP and the transversal momentums p_x and p_y (Eq. (1.3)) describe the beam widen or focusing. For an easier handling and clear represented value of the longitudinal beam momentum p_z , the energy derivation δ (Eq. (1.2)) get introduced.

The definition of these variables may vary by some constants in different literature, but the meaning and physical representation still remains the same.

Frenet-Serret Coordinates

The FSC is a coordinate system which origin refers to the moving object, i. e. the RP, using the normal, binormal and tangent derivative of the trajectory as unit vectors. The other particles can now be described in relation to this idealistic particle.

This coordinate system has the advantage to provide an elegant description of the beam parameter even in curved trajectory as in a synchrotron (ring), cyclotron (spiral) or bunch compressor (chicane) in which parameters in the Cartesian coordinate system seems more cumbersome to handle.

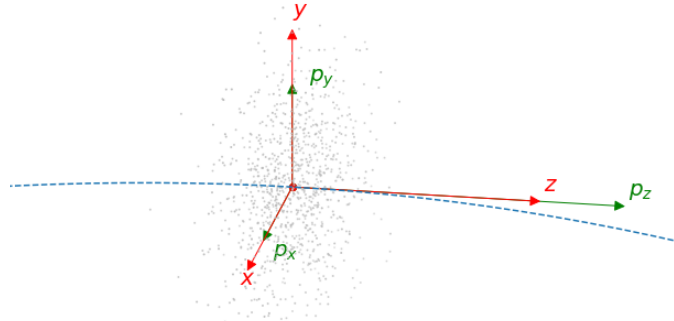


Figure 1.1: Frenet-Serret Coordinates; Where the red centered dot represents the RP, which moves along the blue dotted reference trajectory and defines the orientation of the red spatial axis. The green axes indicate the direction of the momenta (p_x and p_y of the RP = 0). Where the gray dots symbolize other particles of the bunch.

Particle Bunch

Sigma Matrix In order to describe the whole particle bunch in a compact form, the Sigma Matrix (Σ) provides a handy representation. Here, the correlation between each particle parameter v get summarized in one Matrix.

$$\Sigma_{ij} = \langle (v_i - \langle v_i \rangle)(v_j - \langle v_j \rangle) \rangle = \langle v_i v_j \rangle - \langle v_i \rangle \langle v_j \rangle \quad i, j \in \{x, y, z\} \quad (1.4)$$

The $\langle \cdot \rangle$ operator denotes the overall mean, defined as $\langle v_i \rangle \equiv \frac{1}{N} \sum_{n=1}^N v_{i,n}$, where N is the total number of particles. This definition leads to the symmetric matrix:

$$\Sigma = \begin{pmatrix} \langle x^2 \rangle & \langle xp_x \rangle & \langle xy \rangle & \langle xp_y \rangle & \langle xz \rangle & \langle x\delta \rangle \\ \langle px \rangle & \langle p_x^2 \rangle & \langle p_xy \rangle & \langle p_x p_y \rangle & \langle p_x z \rangle & \langle p_x \delta \rangle \\ \langle yx \rangle & \langle yp_x \rangle & \langle y^2 \rangle & \langle yp_y \rangle & \langle yz \rangle & \langle y\delta \rangle \\ \langle py \rangle & \langle py p_x \rangle & \langle py y \rangle & \langle py^2 \rangle & \langle py z \rangle & \langle py \delta \rangle \\ \langle zx \rangle & \langle zp_x \rangle & \langle zy \rangle & \langle zp_y \rangle & \langle z^2 \rangle & \langle z\delta \rangle \\ \langle \delta x \rangle & \langle \delta p_x \rangle & \langle \delta y \rangle & \langle \delta p_y \rangle & \langle \delta z \rangle & \langle \delta^2 \rangle \end{pmatrix}. \quad (1.5)$$

This representation also provides an easy way to identify dependencies in between the three orthogonal planes. Defining σ_i as a (2×2) Matrix.

$$\sigma_i = \begin{pmatrix} \langle i^2 \rangle & \langle ip_i \rangle \\ \langle p_i i \rangle & \langle p_i^2 \rangle \end{pmatrix} \quad i = x, y, z \quad (1.6)$$

An Σ in the block diagonal as in Eq. (1.7) is considered as uncoupled, because no correlations in between the canonical pairs exist. Any matrix entry outside of these arranged sub matrices "couples" the beam.

$$\sigma = \begin{pmatrix} \sigma_x & 0 & 0 \\ 0 & \sigma_y & 0 \\ 0 & 0 & \sigma_z \end{pmatrix} \quad (1.7)$$

TWISS - Parameter If the beam is uncoupled, for example provided by a synchotron or sufficient decoupling optics, the beam can be described with the Twiss-, also known as Courant-Snyder-, parameter. Due to the uncoupled property the different planes do not influence each other, so they get handled separately.

Considering σ_i analogous to Eq. (1.6), the (2×2) sub matrix now gets represented as:

$$\sigma_i = \begin{pmatrix} \beta_i & -\alpha_i \\ -\alpha_i & \gamma_i \end{pmatrix} \cdot \varepsilon_i \quad i = x, y, z \quad (1.8)$$

These Twiss parameter provide a good way to describe the elliptical shape of the phase space in each plane, where α can be interpreted as the tilt of the ellipse and β , the so called "envelope function", describes the ratio of the ellipse axes. γ is a on α and β dependent property $\gamma = \frac{1+\alpha^2}{\beta}$. ε is the beam emittance, the bunch volume in the six dimensional phase space, which not only describes the scaling of the ellipse but also is a quantity for the beam quality. The beam line elements change the form and tilt of the ellipse.

The particles rotate in the phase space along the ellipse. This angular movement in between two points s_1 and s_2 get described phase shift μ . This quantity can be calculated from the envelope function β .

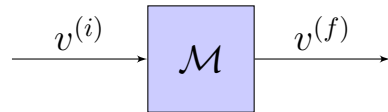
$$\mu_i = \int_{s_1}^{s_2} \frac{1}{\beta_i} ds \quad i = x, y, z \quad (1.9)$$

If the beam line is a closed, the betatron tune ν plays an important role to avoid unstable resonances. It is defined by Eq. (1.10), where μ^* denotes the phase shift of one complete turn. The closer ν is to a natural number or a rational number with small numbers in the dividend and divisor, the higher is the chance to meet an unwanted resonance.

$$\nu_i = \frac{\mu_i^*}{2\pi} ds \quad i = x, y, z \quad (1.10)$$

1.2.2 Basic Idea of Map Tracking

In map tracking, each element gets represented by a so called transfer map, which describes its effect on the beam. To calculate the final particle properties ($v^{(f)}$) the map (\mathcal{M}) just has to be applied on the initial particle properties ($v^{(i)}$), as in Eq. (1.11). This procedure is well known and also used in other fields as for example in light optics.



$$v^{(f)} = \mathcal{M} \circ v^{(i)} \quad (1.11)$$

Note, that in this thesis the calligraphic \mathcal{M} represents a nonlinear map and the "normal" M the linear transfer map.

Due to the known positions of the beam line elements, the position of the reference particle s is the preferred choice, in contrast to the energy dependent description using the time t , for an independent variable.

This map formalism brings advantages in the mathematical handling, beam line analysis and can in some also decrease the computational time in relation to time dependent Particle Tracking (tdPT) algorithms.

In order to track the whole bunch in a fast manner, the transfer map can also be applied on Σ itself. Due to the terminology, calling the entries of the Σ moments, this procedure is known as moment tracking. In this case, the operation is as followed.

$$\Sigma^{(f)} = M \circ \Sigma^{(i)} \circ M^T \quad (1.12)$$

Where the (i) indicates the initial and (f) the final state. Note that here the M represents a linear transfer map and M^T its transposed. It is also possible to track with higher order maps \mathcal{M} , but in that procedure just artificial momentums without an physical meaning would get unnecessarily calculated.

Time dependent Particle Tracking

As an alternative to MT , tdPT is established method in accelerator physics. Here the particle get tracked in discrete time steps trough electric and magnetic vector fields. At each of those steps, the deflection gets calculated (Eq. (1.13)), which forms the basis to find the particle position and the parameters for the propagation to the next step. Here time step size, plays an important role for the simulation outcome, because in between those steps, the particle moves linearly according to its momentum.

$$\frac{d\vec{p}}{dt} = q(\vec{v} \times \vec{B} + \vec{E}) \quad (1.13)$$

Due to the implementation tdPT programs do not provide maps for a beam line analysis or the possibility to accumulate the beam line elements. Latter point can lead to high simulation times, especially in repetitive systems.

1.2.3 Hamiltonian Mechanic

Hamiltonian mechanics are a different mathematical way of describe mechanical systems. In this approach the system gets defined by a so called Hamiltonian H , which in most cases refers on the total system energy. This time dependent Hamiltonian can now be used to determine the behavior of the system, using Eq. (1.16) the Hamiltonian equations.

$$H := H_{(\vec{q}_{(t)}, \vec{p}_{(t)})} \quad (1.14)$$

$$H = T_{(\vec{p})} + V_{(\vec{q})} \quad (1.15)$$

$$\frac{d\vec{p}}{dt} = -\frac{\partial H}{\partial \vec{q}} \quad \frac{d\vec{q}}{dt} = \frac{\partial H}{\partial \vec{p}} \quad (1.16)$$

Where \vec{p} denotes the momentum and \vec{q} the position, which relate to the kinetic and potential Energy ($T_{(\vec{p})}$ and $V_{(\vec{q})}$).

Map tracking finds its origin in the Hamiltonian mechanic. The basic idea is to transform the Hamiltonian H in a form in which it describes the six canonical variables v (Eq. (1.1)) with the independent variable s . The canonical pairs get now formed in each plane from the spatial $\vec{q} = x, y, z$ and momentum $\vec{p} = p_x, p_y, \delta$ coordinates as in Eq. (1.17).

$$H := p_z \quad (x, p_x) \quad (y, p_y) \quad (s, \delta) \quad (1.17)$$

1.2.4 Creation of Hamiltonians

Magnetic Interaction

This section focuses on the determination of the magnetic vector field $\vec{B}_{(s)} = (B_x, B_y, B_z)^T$ along the design path and its effect on the particle.

Multipole Expansion The multipole expansion provides a straight forward way to calculate the magnetic field inside of magnets.

$$B_y + iB_x = \sum_{n=0}^{\infty} (ia_n + b_n) \cdot \left(\frac{x+iy}{r_0} \right)^n \quad (1.18)$$

The magnetic field gets described with $\vec{B} = (B_x, B_y)^T$, where a and b represent the skew and "normal" magnetic field on the pole. r_0 is element aperture and n is the number of magnetic pairs -1 .

For an ideal multipole the coefficients a_n and b_n are zero for all, except for one n , so the element has pure $n+1$ -pole properties.

$$B_y + iB_x = \underbrace{(ia_0 + b_0)}_{Dipole} + \underbrace{(ia_1 + b_1) \cdot \left(\frac{x+i \cdot y}{r_0} \right)}_{Quadrupole} + \underbrace{(ia_2 + b_2) \cdot \left(\frac{x^2 - y^2 + i \cdot 2xy}{r_0^2} \right)}_{Sextupole} + \dots \quad (1.19)$$

Keeping in mind, that this expansion neglects the fringe fields ("hard edge model") and assumes plane pole faces, which can lead to necessary modifications for the field before and after the magnet.

Vector Potential The magnetic analogy to the electric potential is the vector potential \vec{A} . It mandatory in the creation of the Hamiltonian for the description of the general canonical momentum.

$$\vec{B} = \nabla \times \vec{A} \quad (1.20)$$

The combination of the multipole expansion (1.18) with the vector potential (1.20) leads to

$$B_y + iB_x = -\frac{\partial A_z}{\partial x} + i \frac{\partial A_z}{\partial y}. \quad (1.21)$$

$$A_x = 0 \quad (1.22)$$

$$A_y = 0 \quad (1.23)$$

$$A_z = -\operatorname{Re} \left(\sum_{n=0}^{\infty} (ia_n + b_n) \cdot \frac{(x+iy)^{n+1}}{nr_0^n} \right) \quad (1.24)$$

It can been seen, that in the multipole expansion just an longitudinal vector potential component exists. This is a direct result of the hard edge model with no pole face rotation, since then the longitudinal magnetic field is considered zero.

The vector potential affects the particle momentum according to the definition of the general canonical momentum. [7, Chapter 20]

$$\vec{P}_i = \vec{p} + e\vec{A} \quad (1.25)$$

Relativistic Hamiltionian

For the construction of a beam line element Hamiltonian, we need to consider the relativistic definition of the kinetic energy T , using the general canonical momentum, and the - in this application electric - potential V .

$$T_{(\vec{p})} = \sqrt{(\vec{p}c)^2 + (mc^2)^2} \quad \vec{p} = (\vec{P} - e\vec{A}) \quad (1.26a)$$

$$V_{(\vec{q})} = e\Phi_{(\vec{q})} \quad (1.26b)$$

Applying those definitions with Eq. (1.15) leads to the origin for the map creation.

$$H_{(t)} = e\Phi + \sqrt{\left((\vec{P} - e\vec{A})c\right)^2 + (mc^2)^2} \quad (1.27)$$

In this form, the Hamiltonian uses different dependent variables as in (1.1) and the time t as independent variable. Furthermore it is not generalized for curved trajectories, as in a dipole. These three differences require each an canonical transformation to change the Hamiltonian variables to the wanted form as in Eq. (1.17) and general for curvature (attached in Sec. "Canonical Transformations"). These transformations result in Eq. (1.28) for a straight and Eq. (1.29) for a curved trajectory.

$$H = \frac{\delta}{\beta_0} - \sqrt{\left(\frac{1}{\beta_0} + \delta - \frac{q\Phi}{P_0 c}\right)^2 - (p_x - a_x)^2 - (p_y - a_y)^2 - \frac{1}{(\beta_0 \gamma_0)^2} + a_s} \quad (1.28)$$

$$H = \frac{\delta}{\beta_0} - (1 + hx) \sqrt{\left(\frac{1}{\beta_0} + \delta - \frac{q\Phi}{P_0 c}\right)^2 - (p_x - a_x)^2 - (p_y - a_y)^2 - \frac{1}{(\beta_0 \gamma_0)^2} + (1 + hx) a_s} \quad (1.29)$$

Where the vector potential is normalized according to Eq. (1.30) and the momentum to Eq. (1.3).

$$a_i = \frac{A_i}{qP_0} \quad i = x, y, s \quad (1.30)$$

Hamiltonians of beam line elements

In this section previous formulas get combined to form the Hamiltonian for the different beam elements. All of those build up on Eq. (1.28) for a straight and Eq. (1.29) for curved trajectory.

Drift Space A drift space represents a field free beam line section. The vector and electrical potential are zero and lead to a following Hamiltonian:

$$H_{Drift} = \frac{\delta}{\beta_0} - \sqrt{\left(\frac{1}{\beta_0} + \delta\right)^2 - p_x^2 - p_y^2 - \frac{1}{(\beta_0 \gamma_0)^2}}. \quad (1.31)$$

Dipole The dipole is an element with a curved trajectory. Its only field is magnetic, which leads to an longitudinal vector potential A_s . For a description of the magnetic field B_0 relative on the beam, it gets normalized with the inverse magnetic beam rigidity to k_0 .

$$A_s = \frac{b_0}{r_0 P_0} \left(x - \frac{hx^2}{2(1+hx)} \right) \quad (1.32)$$

$$k_0 = \frac{b_0}{r_0 P_0} \quad (1.33)$$

$$H_{Dipole} = \frac{\delta}{\beta_0} - (1+hx) \sqrt{\left(\frac{1}{\beta_0} + \delta\right)^2 - p_x^2 - p_y^2 - \frac{1}{(\beta_0 \gamma_0)^2}} + (1+hx) k_0 \left(x - \frac{hx^2}{2(1+hx)} \right) \quad (1.34)$$

Dipole - Pole Face Rotation An exit or entrance pole face rotation would lead to an additional magnetic field at the magnet ends.

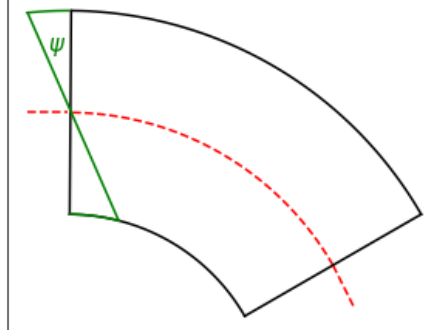


Figure 1.2: Pole Face Rotation; In this figure, the black line represents a dipole magnet with orthogonal edges. The green magnet edge is a pole face rotation of the angle Ψ , where the red dotted line indicates the reference trajectory.

Those fields can get described with Eq. (1.35a). Hence the occurring longitudinal magnetic field leads to a vector potential in the dispersion plane a_x .

$$B_x = -B_0 \frac{y}{l} \tan(\Psi) \quad (1.35a)$$

$$B_y = B_0 \left(\frac{\xi}{l} - \frac{x}{l} \tan(\Psi) \right) \quad (1.35b)$$

$$B_s = B_0 \frac{y}{l} \quad (1.35c)$$

Wheres ξ represents the longitudinal position in the entrance or exit fringe field, which has the length l . Deriving the normalized vector potentials lead to Eq. (1.36). Due to the already second order of y in a_x the quadratic general canonical momentum therm in the x-plane is of the 4th order. This would result in additional 3rd order effects in the y-plane on the particle bunch.

$$a_x = \frac{1}{2} \frac{k_0}{l} (\xi^2 - y^2) \quad (1.36a)$$

$$a_s = -\frac{1}{2} \frac{k_0}{l} (y^2 - x^2) \tan(\Psi) \quad (1.36b)$$

For a linear approximation just gets a_s considered. The form of this potential is similar to the quadrupole vector potential. Which make it possible to handle this potential independently as a fictional quadrupole. Using a "thin lens approximation" results in a Hamiltonian according to (1.37) with the form of a "Kick Map". These maps can now be added before and after the "pole face rotation free" dipole to get a linear approximation for the pole face rotation.

$$H_{ThinLens} = \frac{1}{2} (x^2 - y^2) k_0 \tan(\Psi) \quad (1.37)$$

Quadrupole The Hamiltonian of a quadrupole is created using Eq. (1.28) and Eq. (1.22) with $n = 1$ for the vector potential . For a simplified representation, k_1 gets introduced which represents the normalized field gradient.

$$A_s = \frac{1}{2} \frac{b_1}{r_0} (x^2 - y^2) \quad (1.38)$$

$$k_1 = \frac{b_1}{r_0} \frac{q}{P_0} \quad (1.39)$$

$$H_{Quadrupole} = \frac{\delta}{\beta_0} - \sqrt{\left(\frac{1}{\beta_0} + \delta \right)^2 - p_x^2 - p_y^2 - \frac{1}{(\beta_0 \gamma_0)^2}} + \frac{1}{2} k_1 (x^2 - y^2) \quad (1.40)$$

1.2.5 Truncated Power Series Algebra

The idea of a DA is to "solve analytic problems with algebraic means". DA are a method to bring functions and operations on them in a for the computer treatable form, similar to numbers [2, Chapter 2]. The TPSA is a special form of a DA. Here the Taylor expansion \mathcal{T} is used as equivalence relation, which transforms numbers and functions in truncated polynomials Eq. (1.42).

$$f := f_{(\vec{v}_{(s)})} \quad (1.41)$$

$$f = \mathcal{M} \Leftrightarrow \sum_{n=0}^{\Omega} \underbrace{\frac{f^{(n)}}{n!}}_{\text{Taylor series}} (\vec{v}_{(\Delta s)})^n + \underbrace{\mathcal{O}(\vec{v}_{(\Delta s)}^{\Omega+1})}_{\text{error therm}} \quad (1.42)$$

Where $f_{(\vec{v}_{(s)})}$ is a general function on the particle parameter, which acts similar to an element map \mathcal{M} . This map can be represented equivalently in a Taylor series \mathcal{T} of f .

Right away from the definition in Eq. (1.42) it can be seen, that this approach needs to have an $\Omega \rightarrow \infty$ to transform the original function precisely. In reality, these series get truncated at a certain order, which leads to the error therm $\mathcal{O}(\vec{v}_{(\Delta s)}^{\Omega+1})$. The physical role of this error therm has an important meaning in context of the precision or the symplecticity of the map, which gets discussed later.

In order to handle these polynomials, the TPSA defines own operations, even the derivative, to act consistent to in the classical algebra (Fig. 1.3).

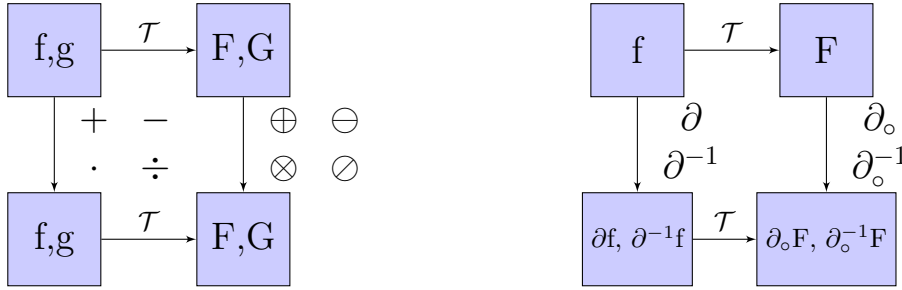


Figure 1.3: Graphical representation of DA and its operators.

In this flow chart representation the functions $f, g \in C^\infty$ where $f : [a, b] \subset \mathbb{R}^V \rightarrow \mathbb{R}$. The lower case characters, on the left side, symbolize the function in the classical analytical space and the upper, on the right side, case represent the same (transformed) functions in the DA. In TPSA \mathcal{T} denotes the multidimensional Taylor Series Operator.[2]

Considering, that the maximal number of possible monomials depends on the dimension ν and the truncation order n , its behave according to the binomial coefficient in (1.43).

$$K = \binom{n + \nu - 1}{\nu - 1} = \frac{(n + \nu - 1)!}{n! (\nu - 1)!} \quad (1.43)$$

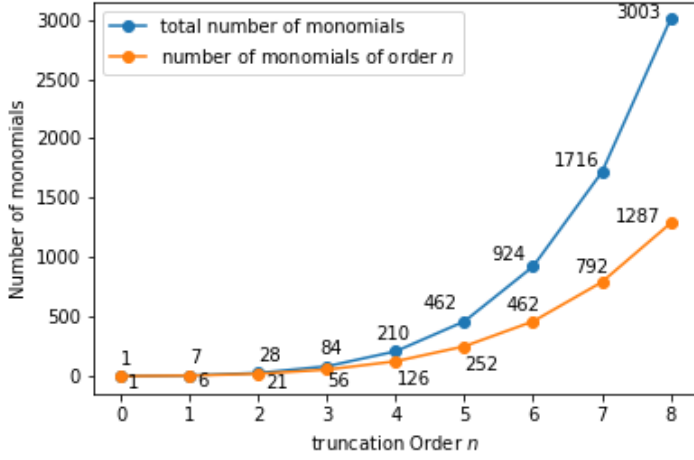


Figure 1.4: Number of monomials in nD_6 ; the orange line represents the number of monomials of order n and the blue line the total number.

1.2.6 Map Creation - Lie Algebra

The application of the Lie Algebra in accelerator physics gets introduced by Dragt in [8]. In its principle the Lie Operator Eq. (1.45) and the Lie Transformation Eq. (1.46) get defined.

$$f := f_{(q_{(\vec{s})}, p_{(\vec{s})})} \quad (1.44)$$

$$:f := [f, \circ] = \sum_{i=1}^n \left(\frac{\partial f}{\partial q_i} \frac{\partial \circ}{\partial p_i} - \frac{\partial f}{\partial p_i} \frac{\partial \circ}{\partial q_i} \right) \quad (1.45)$$

$$e^{:f:} = \sum_{k=0}^{\infty} \frac{1}{k!} :f:^k = 1 + :f: + \frac{1}{2} :f:^2 + \dots \quad (1.46)$$

$$(1.47)$$

In other words:

"A Lie Operator is a Poisson bracket, waiting to happen." - Volker Ziemann

Assuming total derivative of the function f :

$$\frac{df}{ds} = \sum_{i=1}^{n/2} \left(\frac{dq_i}{ds} \frac{\partial f}{\partial q_i} + \frac{dp_i}{ds} \frac{\partial f}{\partial p_i} \right) \quad (1.48)$$

Where q_i and p_i are the canonical, spatial and momentum, pairs. Combining this total derivative with Hamilton's equations of motions (Eq. (1.16)) leads to the following relation.

$$\frac{df}{ds} = \sum_{i=1}^n \left(\frac{\partial H}{\partial p_i} \frac{\partial f}{\partial q_i} - \frac{\partial H}{\partial q_i} \frac{\partial f}{\partial p_i} \right) \equiv -:H:f \quad (1.49)$$

Solving this differential equation while assuming f describes the beam parameter, the map \mathcal{M} can get extracted.

$$f_{(s)} = e^{-H \cdot s} f_{(s_0)} \quad (1.50a)$$

$$\mathcal{M} = e^{-H \cdot s} \quad (1.50b)$$

Due to the distributivity of Lie operator, it is possible to decide up to which order the effects get observed. This can be done in simply truncating the Lie transformation Eq. (1.46) after the wanted therm.

$$\mathcal{M} = \underbrace{e^{H_0}}_{\text{centroid}} \cdot \underbrace{e^{H_1}}_{\text{Quadrupole}} \cdot \underbrace{e^{H_2}}_{\text{Sextupole}} \cdot \underbrace{e^{H_3}}_{\text{Octupole}} \cdot \dots \quad (1.51)$$

The separation of H in its orders H_i , where $i = 0, 1, 2, 3, \dots$, illustrates the determination of effects in the according orders. Furthermore, it also points the symplectic nature of each map out [8, Chapter 7.1.].

1.2.7 Map Analysis

This section is widely extracted out of Wolski's publication [9]. These calculations may seem extensive and sometimes bear the problem of the reassignment of matrix eigenvalues/-vectors to the according plane, but they are a general approach and can also be applied on coupled beam /-lines.

One of the advantages of map tracking is the stored information in each transfer map M . These linear maps contain information about the beam line as stability and symplecticity. To get characteristics about the bunch, as the beam emittance, the Σ has to get analyzed. A comparison of the two matrices show the match of the bunch to the beam line.

Sigma Matrix Σ

The Sigma matrix Σ , not only contains information about the beam coupling, but also about its emittance ε . This information is stored in eigenvalues of the accumulated $\Sigma \circ S$ Matrix, where S is the Skew matrix [9, Section III.B.].

$$S = \begin{pmatrix} S' & 0 & 0 \\ 0 & S' & 0 \\ 0 & 0 & S' \end{pmatrix} \quad S' = \begin{pmatrix} 0 & 1 \\ -1 & 0 \end{pmatrix} \quad (1.52)$$

$$\varepsilon_x = i \lambda_{1,2} \quad (1.53a)$$

$$\varepsilon_y = i \lambda_{3,4} \quad (1.53b)$$

$$\varepsilon_z = i \lambda_{5,6} \quad (1.53c)$$

Transfer Matrix

The transfer matrix contains diverse information about the beam line (element), as

1. Coupling
2. Stability & Symplecticity
3. Phase Shift (\rightarrow tune).

Coupling Analogous to Σ , all elements in \mathbf{M} outside of the (2×2) diagonal blocks lead to a beam coupling. Considering higher order maps, this rule applies on every monomial containing elements of two different canonical pairs. These terms not only couple the beam, but also can be used to decouple it.

Dispersion The dispersion are represented in the linear transfer matrix \mathbf{M} at $\eta_x = m_{1,6}$, $\eta_{px} = m_{2,6}$, $\eta_y = m_{3,6}$ and $\eta_{py} = m_{4,6}$, where in $m_{i,j}$ i denotes the row and j the column index in \mathbf{M} . These terms can lead to chromatic aberrations as in a beam widening η_{pi} , while creating an energy deviation along the dispersal axis η_i . In the first order such terms occur in the bending plane of dipole maps. In higher orders those effect get described by the monomials containing δ . In quadrupoles they already occur in the second order.

This effect may be unwanted in some applications as in gantries, but it also gets used in energy spectrometer or energy selection systems.

Stability & Symplecticity The stability gets extracted by the absolute value of the transfer map eigenvalues. Considering the definition of eigenvalues, its absolute value unequal to one would mean an stretch or compression along the according eigenvector. In a visualization, the eigenvalues have to lie on the unit circle, the argument needs to be $|\lambda| = 1$. Every different value lead to a manipulation of the beam emittance along the according eigenvector and lead to an unstable beam behavior.

$$\mathbf{M}\lambda = \vec{e}\lambda \quad (1.54)$$

The symplecticity describes the conservation of the beam emittance. It gets defined in

$$\mathbf{M}^T \mathbf{S} \mathbf{M} = \mathbf{S}, \quad (1.55)$$

where \mathbf{M} is the symplectic map and \mathbf{S} represents the skew matrix form Eq. (1.52).

Neglecting this criteria lead to a violation of the Hamiltonian model itself. In ring beam lines, i. e. synchrotrons, is this criteria of highest importance. For long time simulations in storage rings, the map can even get adjusted, to the cost of its precision, full fill this symplecticity criteria [10].

Phase Shift There are several ways to calculate the phase shift. In the following, two ways for an coupled beam get introduced.

Phase Shift with Eigenvalues In symplectic maps the eigenvalues always occur in complex eigenvalue pairs $\lambda_{\pm k}$. Its value can be interpreted by

$$\lambda_{\pm k} = e^{\pm 2\pi i \nu_k} \quad k = x, y, z. \quad (1.56)$$

Using Euler's formula leads to following form:

$$\exp^{\pm ix} = \cos(x) \pm i \sin(x) \quad (1.57)$$

$$\lambda_{+k} + \lambda_{-k} = 2 \operatorname{Re}(\lambda_{+k}) = 2 \cos(2\pi\nu_k) \quad (1.58)$$

$$\nu_k = \frac{1}{2\pi} \arccos(\operatorname{Re}(\lambda_{+k})) \quad (1.59)$$

In this derivation, the betatron tune gets denoted with ν . The phase shift μ can now get extracted according to following relation.

$$\mu_k = 2\pi\nu_k \quad k = x, y, z \quad (1.60)$$

Phase Shift using Rotation Matrix In this approach a rotation matrix \mathbf{R} gets introduced, which contains easily extractable information about the phase shift μ .

$$\mathbf{R}_{(\mu_x, \mu_y, \mu_z)} = \begin{pmatrix} \mathbf{R}_{2(\mu_x)} & 0 & 0 \\ 0 & \mathbf{R}_{2(\mu_y)} & 0 \\ 0 & 0 & \mathbf{R}_{2(\mu_z)} \end{pmatrix}, \quad \mathbf{R}_{2(\alpha)} = \begin{pmatrix} \cos(\alpha) & \sin(\alpha) \\ -\sin(\alpha) & \cos(\alpha) \end{pmatrix} \quad (1.61)$$

The creation of \mathbf{R} requires the eigenvector matrix \mathbf{E} of the transfer map \mathbf{M} , which are used to introduce the transformation Matrix \mathbf{N} which acts as a symplectic rotation, thus perseveres the eigenvalues.

If the bunch matches the beam line, as in a synchrotron, \mathbf{R} can get created according to

$$\mathbf{R}_{(\mu_x, \mu_y, \mu_z)} := \mathbf{N}^{-1} \mathbf{M} \mathbf{N}. \quad (1.62)$$

If the bunch missmatches, the calculation is according to Eq. (1.63) and uses additional information from Σ . The creation of two different \mathbf{N} use the data from Σ before and after the map. Furthermore, additional constrains has to be drawn to for \mathbf{N}_1 avoid degeneracy due to the relative property of the phase shift Eq. (1.63).

$$\mathbf{R}_{(\mu_x, \mu_y, \mu_z)} := \mathbf{N}_2^{-1} \mathbf{M} \mathbf{N}_1 \quad (1.63)$$

Transfer and Sigma Matrix

In periodic applications, such as rings, the beam should be invariant to the single turn matrix to be stable.

$$x \rightarrow \mathbf{M}x \quad \Sigma \rightarrow \mathbf{M} \Sigma \mathbf{M}^T = \Sigma \quad (1.64)$$

To conform upper condition, it is necessary that $\Sigma \mathbf{S}$ and \mathbf{M} has the same eigenvectors \mathbf{E} . If those match, the beam is called a "matched distribution".

Chapter 2

Implementations

2.1 OPAL-map

2.1.1 Introduction

OPAL-map is an in the future available map tracking method in the OPAL framework [1]. Its mathematics is based on the map tracking method introduced in Sec. "Basic Idea of Map Tracking".

2.1.2 Flow Chart

As in all OPAL simulations, the system gets defined in the input file, from which the information get split up in the different classes, including for the beam line "OPAL beam line" and the bunch description "particle bunch". OPAL-map now iterates along the beam line elements from "OPAL beam line" and creates the maps for each element or even the slices of them. These get stored in "map beam line". With this data, the maps of the beam line could now be analyzed "map analysis".

In the further steps, the particle data of "particle bunch" get extracted and the maps of "map beam line" applied to track the particle along the beam line. In this loop, the individual particles form the inner and the beam line maps the outer loop. After each slice/ element, the "particle bunch" gets updated and its data finally extracted to the output files.

In the following drawn scheme, the green boxes represent the in- and output, the user interface. The blue boxes symbolize the already implemented OPAL structures and the red show the newly created OPAL-map elements (Fig. 2.1).

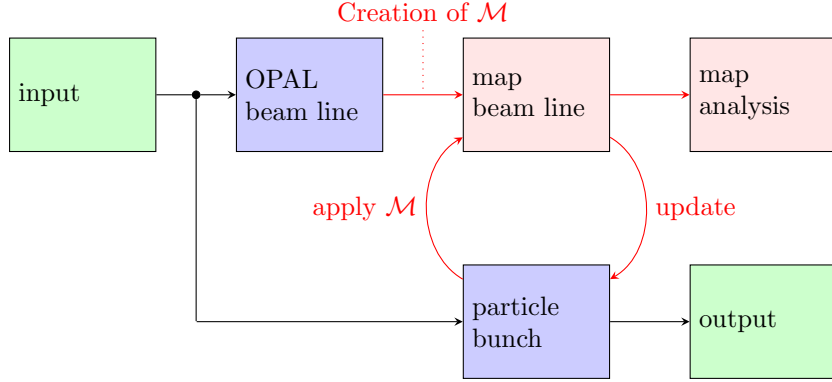


Figure 2.1: OPAL-map flow chart

2.1.3 DA Package

The OPAL Differential Algebra Package [1, DA], bases on TPSA and is used for the map creation. It provides besides the TPSA operations also the multidimensional Taylor expansions for certain functions as for root, exponentiation, fractions and many more. It also contains more specific operations as the Lie transformation.

To keep the computational time as effective as possible, a global truncation order limits the length of the polynomials and so the order of the map. Considering that for a certain map order the Hamiltonian always needs to be one order higher, which can be seen in its Lie algebraic creation.

2.1.4 Map Analysis

The map analysis is done according the theoretical background of Wolski [9] and mentioned in the previous section. For the determination of the eigenvalue and -vectors the the GNU Scientific Library (GSL) [11] were used.

2.2 COSY Infinity

COSY Infinity is a map tracking based beam optics program [12]. It also uses TPSA [2] and therefore provides the possibility to create higher order maps, which were used to verify the OPAL-map maps.

Important to know, is that COSY Infinity and OPAL-map use different constants. COSY Infinity uses the atomic mass in amu and calculates to the energy. This is a reasonable method, but results in too many digits and differs form the constant table (Tab. 2.1).

Program	Proton [$\frac{\text{MeV}}{c^2}$]	Electron [$\frac{\text{MeV}}{c^2}$]
OPAL-map	938.2720813(58)	0.5109989461(31)
COSY Infinity	938.27199893682...	0.51099890307660...

Table 2.1: The difference in constants of COSY Infinity and OPAL-map

The effect of the constants will be shown and discussed in the results section.

2.3 pyAcceLEGOrator

pyAcceLEGOrator [13] is a python based beam optics code. It used the hard coded algebraic solution to create the linear transfer maps and therefore provides a handy reference to the Lie algebra maps.

Chapter 3

Results

3.1 FODO Cell

In this example, a simple FODO cell gets simulated.

Quantity	Value
particle	Proton
E_{kin}	100 MeV

The Quadrupole settings:

Name	Field Gradient	Length
Q1	8.64195 T/m	0.3m
Q2	-11.57456 T/m	0.3m
Q3	8.64195 T/m	0.3m

Table 3.1: Quadrupole settings of FODO cell. This setting was chosen after an 1st order optimization with COSY Infinity.

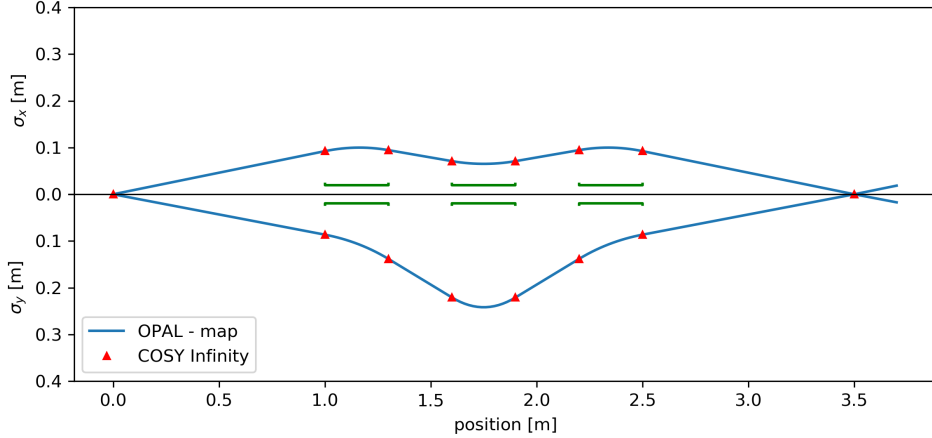


Figure 3.1: "FODO" envelopes plot (1st Order); The blue line represents the envelopes of OPAL-map and the red triangles the data points of COSY Infinity. The green lines indicate the position of the quadrupoles

In Fig. 3.1 the comparison of the COSY Infinity and the OPAL-map envelopes is plotted. The green lines in the plot indicate the quadrupoles, neglecting the aperture and the consequential particle loss. For a better visualization, the envelope of OPAL-map has a continuous line and the data points of COSY Infinity are represented with triangles. It can be seen, that each COSY Infinity data point lies on the element edges, so in the initial position and the end of each map. This demonstrates the advantage of the possible huge step size, with the disadvantage of the lack of information in between.

An example has been chosen to visualize, higher order effects in this small system. For this purpose, a strongly divergent beam containing nine particles was chosen. Defining a transversal momentum of $p_t = \pm 0.15 \frac{p_z}{p_0}$. This momentum gets assigned to the particles in the x and/ or y plane in every possible combination. So a particle have none, one or two transversal momenta, either positive or negative.

In the first simulation Fig. 3.2, the longitudinal momentum of each particle gets adjusted, so that the energy deviation $\delta = 0$.

In a second run Fig. 3.3, the longitudinal momentum of each particle was defined with $p_z = p_0$, ignoring the transversal momenta. This definition leads to an energy deviation $\delta = 5.325 \cdot 10^{-3}$ or $1.064 \cdot 10^{-2}$, depending, if the particle has one or two assigned transversal momenta.

The idea of those two runs can be seen in the x plane of the complete FODO map at the focal point ($s = 3.5\text{m}$, Fig. 3.4), where all the second order thermals have are related to the energy deviation. For the purpose of completeness, the whole transfer matrix gets provided in the appendix B.

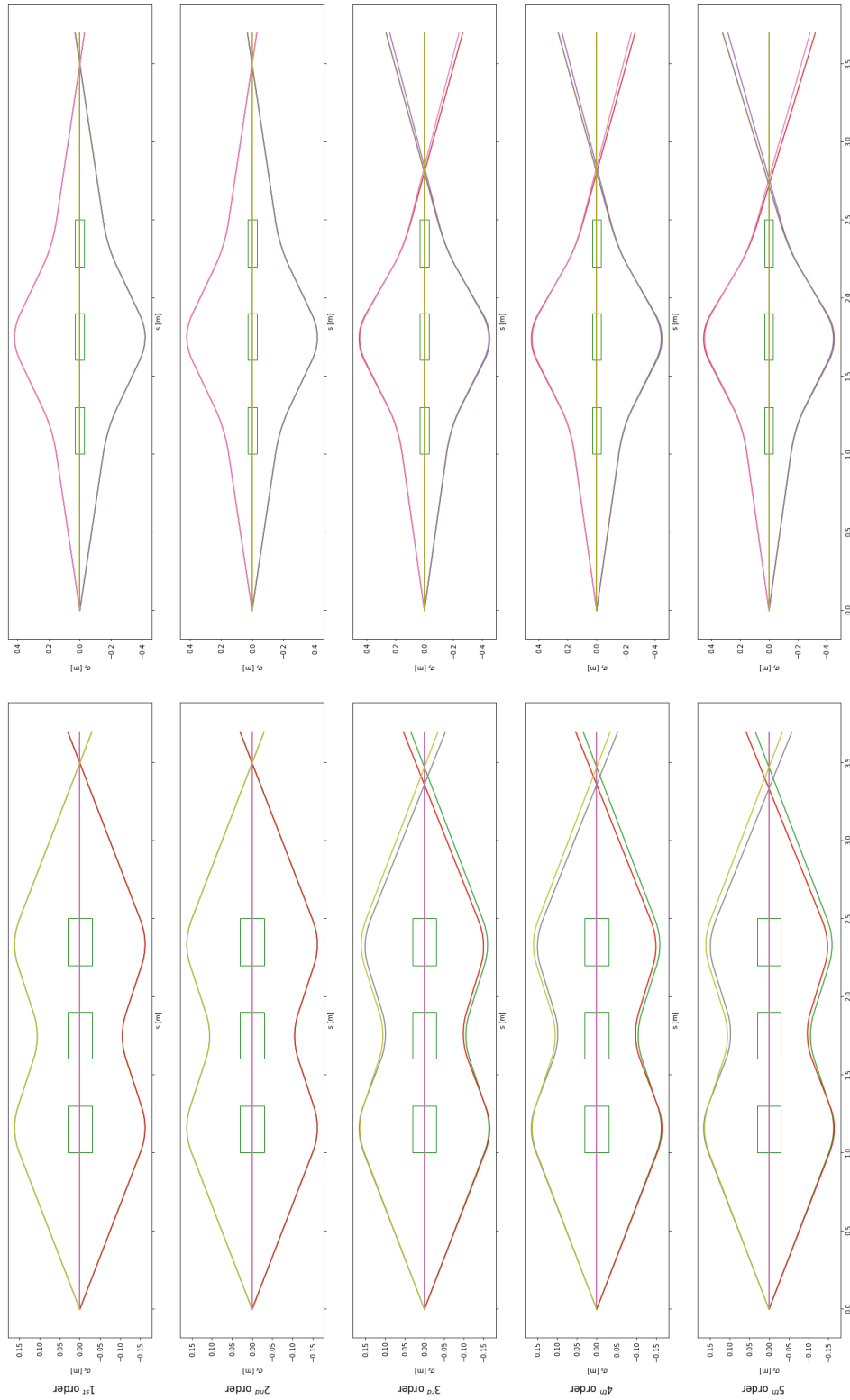


Figure 3.2: FODO with divergent beam and $\delta = 0$; The plots on the left illustrate the envelopes in the x-plane and the one on the right the y-plane. Each row represents a simulation considering the effects of the order denoted on the left.

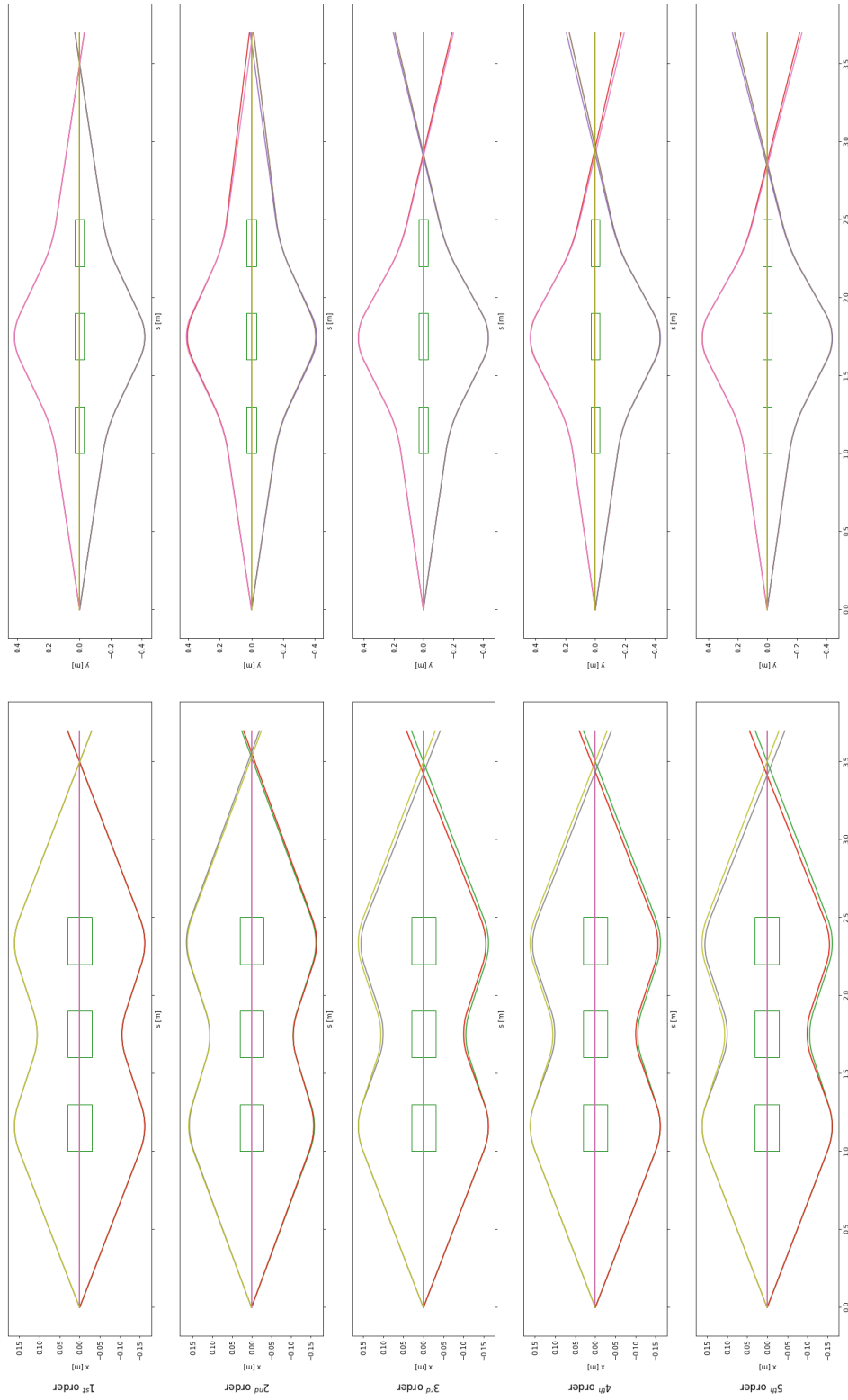


Figure 3.3: FODO with divergent beam and $\delta \neq 0$; The plots on the left illustrate the envelopes in the x-plane and the one on the right the y-plane. Each row represents a simulation considering the effects of the order denoted on the left.

Transfermap FODO						
coefficient	x	px	y	py	z	delta
-1.02619697697268e+00	1	0	0	0	0	0
-1.99970538528579e-01	0	1	0	0	0	0
-7.43993992258748e-01	1	0	0	0	0	1
6.81372414922869e+00	0	1	0	0	0	1
4.24058384937832e-01	3	0	0	0	0	0
-2.01179574465487e+00	2	1	0	0	0	0
1.21249388325331e-01	1	2	0	0	0	0
1.52926590368216e+00	1	0	2	0	0	0
3.42916108688955e+00	1	0	1	1	0	0
1.76109899012140e+00	1	0	0	2	0	0
2.60280764146783e+01	1	0	0	0	0	2
-1.33623600329734e+00	0	3	0	0	0	0
-2.77504233826512e+00	0	1	2	0	0	0
-5.85149886953810e+00	0	1	1	1	0	0
-3.92870468155939e+00	0	1	0	2	0	0
-1.84339358344320e+01	0	1	0	0	0	2

Figure 3.4: The transfer map of the FODO for the x coordinate up to the third order

The big difference between Fig. 3.2 and Fig. 3.3 can be seen in the focus point at $s = 3.5\text{m}$. Considering the first order, both simulations show similar trajectories and a good focus. In higher orders, the two simulations start to differ.

In the first run with no energy deviation $\delta = 0$, the defocussing starts at the 3rd order, in contrast to the second run, where this chromatic aberration already starts at the 2nd order.

The explanation can be seen in the transfer matrix. The 2nd order effects are all related to the energy deviation δ (with x and p_x). There is no additional effect in the first run, because all monomials with $\delta \langle \delta \cdot \rangle = 0$. The 3rd order effects contain various relations also monomials $\langle \cdot \cdot \rangle \neq 0$, so even a beam with no energy deviation starts to defocus.

To analyze the impact of the different particle mass constants in OPAL-map and COSY Infinity, mentioned in Sec. "COSY Infinity", their maps get compared. For that, the absolute difference of the coefficients gets calculated, neglecting a weighting for the monomial order. In the following plot the maximum and the mean difference are shown.

For the separation the influence of the different constants and the map difference itself, the COSY Infinity constants have been used in OPAL-map and its map compared in similar manner.

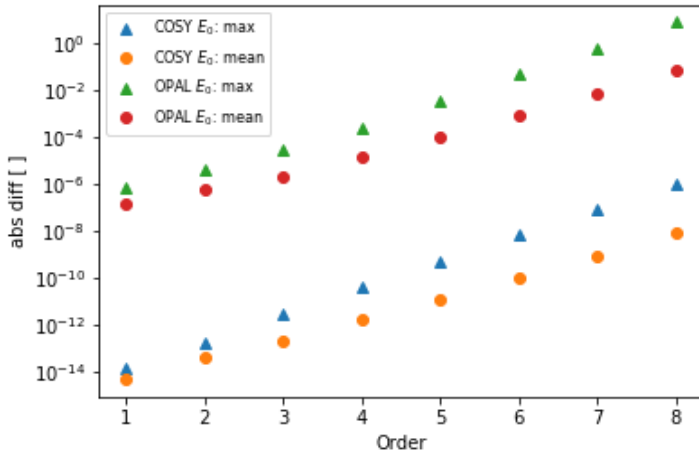


Figure 3.5: "FODO" map comparison; In the plot 2 different scenarios are shown, once OPAL-map uses the same constants for the particle mass E_0 as COSY Infinity (COSY E_0) and once its own (OPAL E_0). Now the value of the mean or the maximal difference (max) of all map coefficients are shown.

3.2 FODO + Dipole

This simulation models a FODO cell of the synchrotron example in following section. Its beam gets defined by:

Quantity	Value
particle	Electron
E_{kin}	999.49 MeV

Table 3.2: Synchrotron electron beam settings

The beam line setting settings:

Name	Field/-gradient	Length
Qf	-10.9409 T/m	0.2m
B1	-2.3287 T/m	
Qd	11.0410 T/m	0.3m
B2	-2.3287 T/m	
Q3	8.6420 T/m	0.3m

Table 3.3: Settings taken from Synchrotron example

The drift length in between all elements is $l = 0.5\text{m}$.

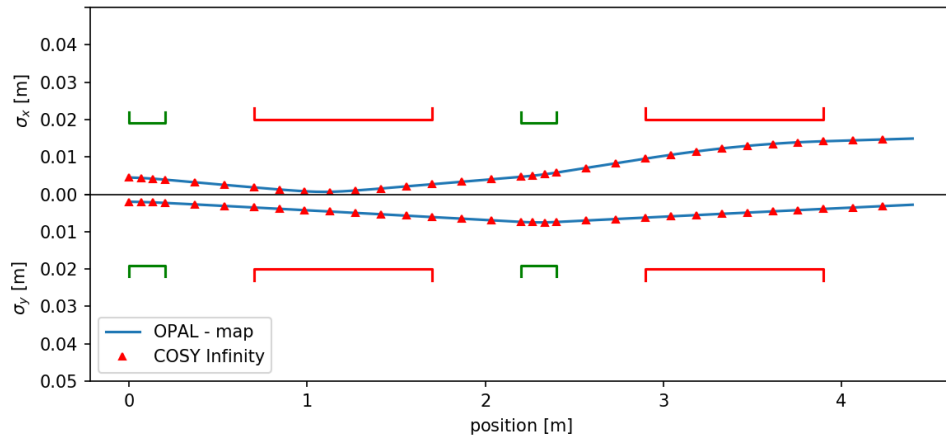


Figure 3.6: "FODO + Dipole" envelopes plot (1st Order); The blue line represents the envelopes of OPAL-map and the red triangles the data points of COSY Infinity. The green lines indicate the position of the quadrupoles, and the red the position of the dipoles

In Fig. 3.6, similar to 3.1, the triangles represent the data points of COSY Infinity. It can be seen here, that COSY Infinity's element maps has been sliced, similar as in OPAL-map, to gain more data points, even inside the elements itself. In this example, the dipoles bend along the y-axis, which makes the x- to the dispersal plane.

A similar map comparison as in Fig. 3.5, has been done, considering a higher beam energy, a lower particle mass and the presence of dipoles.

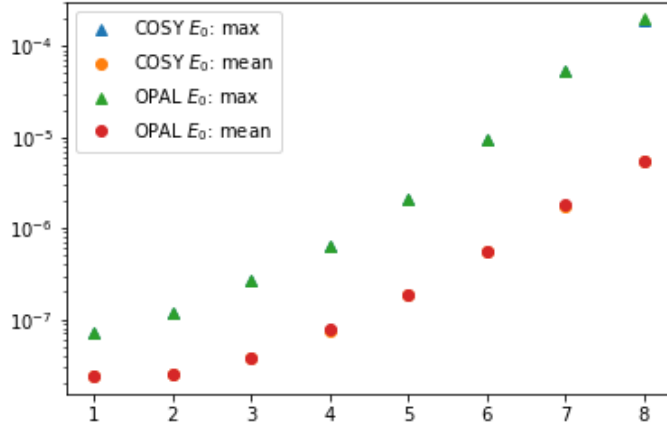


Figure 3.7: "FODO + Dipole" map comparison; In the plot 2 different scenarios are shown, once OPAL-map uses the same constants for the particle mass E_0 as COSY Infinity (COSY E_0) and once its own (OPAL E_0). Now the value of the mean or the maximal difference (max) of all map coefficients are shown.

Here does the error, caused by the different constants, not influence the comparison significantly.

With dipoles in the beam line, the dispersion can be tracked. Since this section was taken out of the synchrotron example from the next section, an initial dispersion η_{x0} was chosen, to match the ring conditions.

Dispersion	Value
η_{x0}	0.5069938765m
η_{p_x0}	-0.1681363086

Table 3.4: Initial Dispersion taken from Synchrotron example

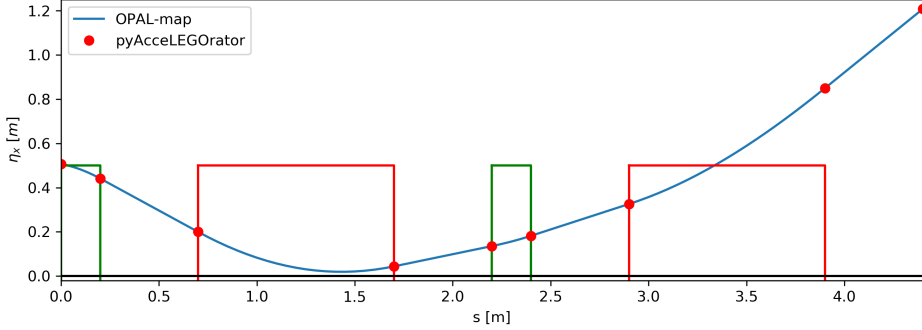


Figure 3.8: "FODO + Dipole" dispersion plot; Here the dispersion along the beam line gets illustrated. The blue line illustrates the simulation in OPAL-map and the red dots the simulation in pyAcceL. The green line indicate the position of the quadrupoles and the red lines of the dipoles.

3.3 Synchrotron

The beam parameter and the beam line setting are similar to previous example "FODO + Dipole" (Tab. 3.2 & Tab. 3.3), which represents a single FODO cell in this ring. The whole beam line setting, also for the irregular section, is provided in the demo scripts of pyAcceL "collider_madx.ipynb".

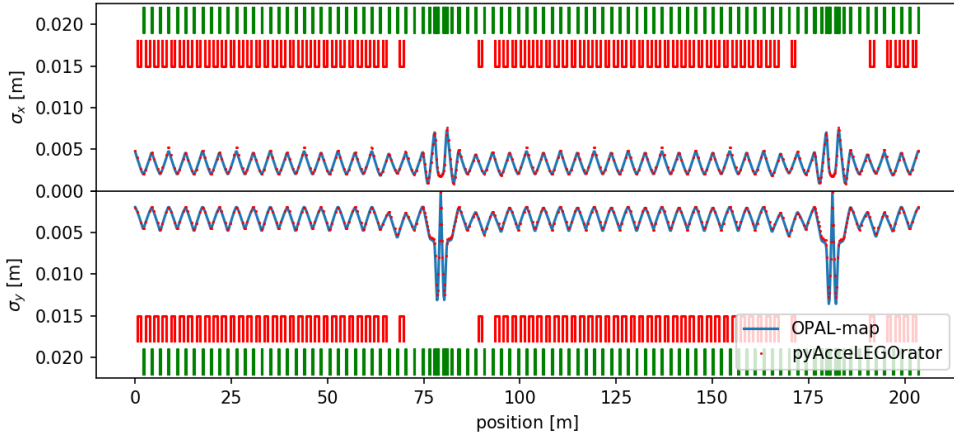


Figure 3.9: Synchrotron envelopes of in 1st order; The blue line shows the OPAL-map and the red dots the pyAcceL simulation. The red elements indicate the dipoles, where the green stand for the dipoles.

In Fig. 3.9 the OPAL-map gets compared to the analytical maps of pyAcceLEGOrator, which data points get represented with red dots.

The eigenvalues of the single turn map provide the betatron tunes ν (Tab. 3.5). The assignment of the eigenvalues to the planes was chosen freely.

Tune	Value
ν_x	$9.610 \cdot 10^{-3}$
ν_y	$2.604 \cdot 10^{-1}$

Table 3.5: Beta tunes of Synchrotron

For the dispersion, the same initial values has been chosen as in the "FODO + Dipole" example (Tab. 3.4), to gain the matched shape.

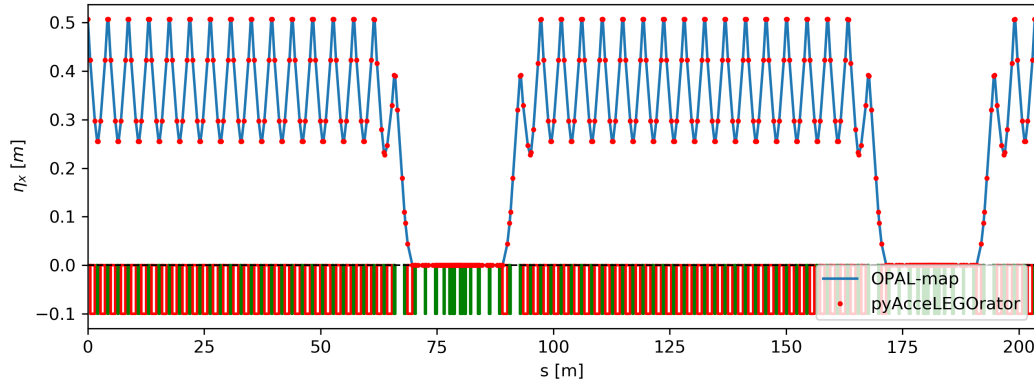


Figure 3.10: Synchrotron dispersion plot; Here the dispersion along the synchrotron ring, simulated with OPAL-map (blue line) and pyAcceL (red dots) is shown. The green lines indicate the quadrupoles and the red the dipoles.

The figure also shows the absence of dispersion in the aperiodic region, which can be used for example the placement of the Radio Frequency (RF) Cavity.

3.4 PSI Gantry 2

The Paul Scherrer Institute (PSI) Gantry 2 is upstream scanning proton therapy gantry with an isocentric layout as in Fig. 3.11.

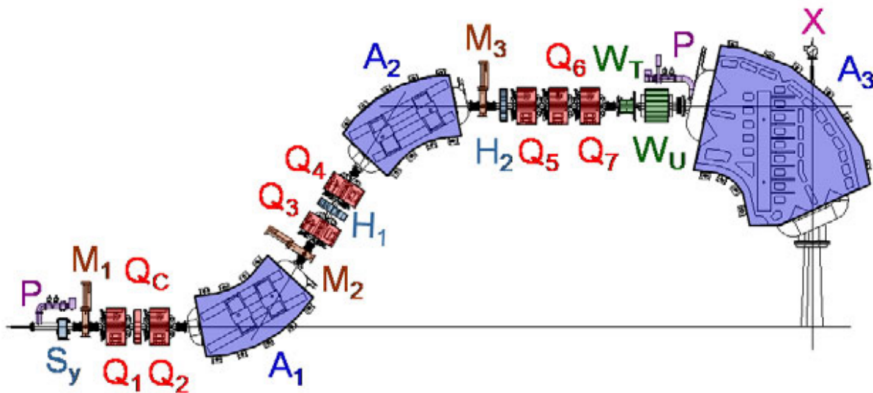


Figure 3.11: Gantry 2 Elements

Symb	Part	Quantity	in OPAL-map
C	collimator	1	not impl.
A	dipole	3	✓
Q	quadrupole	8	✓
H	sextupole	2	deac.
W	scanning magnets	2	deac.
M	monitor	3	✓
S	steering magnet	1	deac.
P	vacuum pump	2	—
X	x-ray source	1	—

The PSI gantry 2 example uses the current beam line setting for 70MeV of the real gantry. Consider, that the sextupole of Gantry 2 are deactivated and for the simulation the sweeper magnets are chosen to not deflect.

Quantity	Value
particle	Proton
E_{kin}	73.81 MeV

Table 3.6: PSI Gantry 2 proton beam settings

This setting represents the lowest energy application, which also has the lowest particle flux due to the degrading process after the cyclotron (COMET). A low flux at a certain energy leads to a low beam intensity, which in turn leads to a low dose rate and a longer treatment time. In proton therapy, longer treatments not only are more expensive, but also limits the usage of sophisticated methods, as breath hold technique or hypo fractionation. [14]

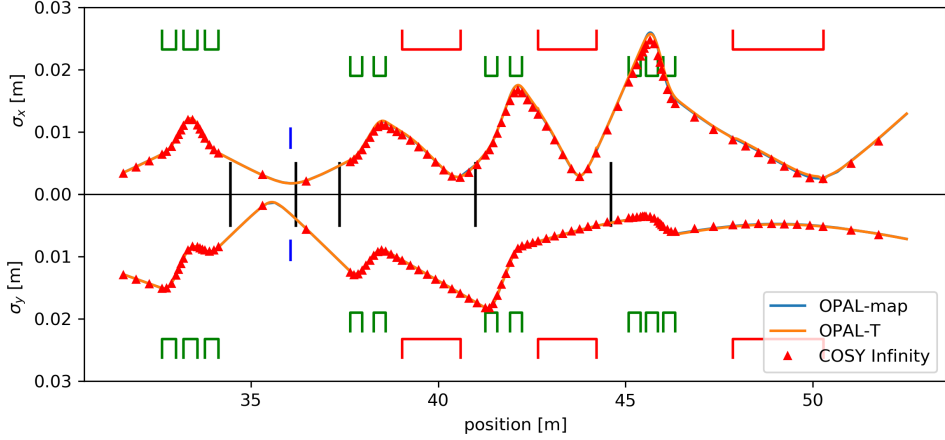


Figure 3.12: PSI gantry 2 envelopes in 1st order (no dipole face pole rotation); The blue line represents the envelopes in the OPAL-map simulation, the orange line OPAL-T and the red triangles COSY Infinity. The green elements represent the quadrupoles and the red elements the dipoles. The black vertical lines indicates the monitor positions, where the blue vertical lines stand for an aperture.

In Fig. 3.12 OPAL-map not only gets compared to COSY Infinity, but also to OPAL-T. The latter is a tdPT based algorithm of the OPAL framework and uses a hard edge model for the fringe fields.

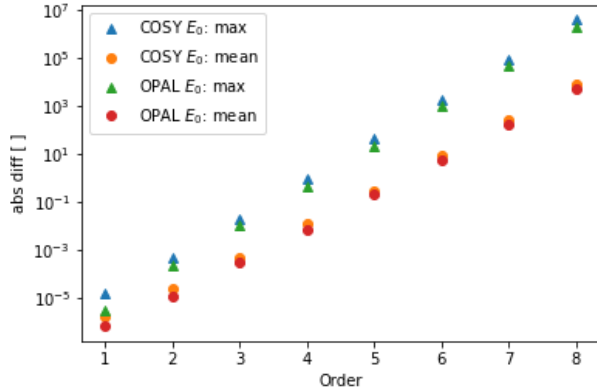


Figure 3.13: PSI gantry 2 map comparison; In the plot 2 different scenarios are shown, once OPAL-map uses the same constants for the particle mass E_0 as COSY Infinity (COSY E_0) and once its own (OPAL E_0). Now the value of the mean or the maximal difference (max) of all map coefficients are shown.

Fig. 3.13 shows the differences in the transfer maps. The plot has been done analogous to the other map comparison Plots, comparing the non weighted coefficients.

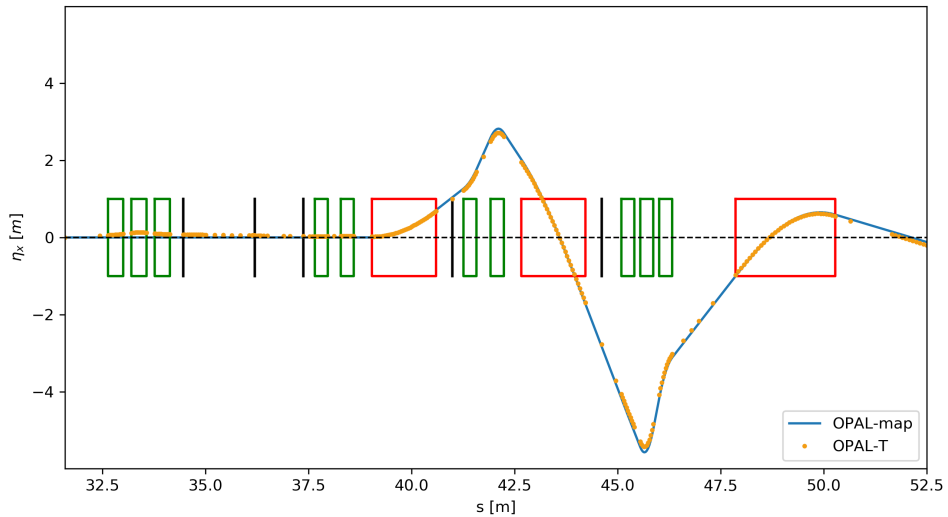


Figure 3.14: PSI gantry 2 Dispersion plot; Here the dispersion along the PSI gantry 2 beam line gets simulated, simulated with OPAL-map (blue line) and OPAL-T (orange dots) is shown. The green lines indicate the quadrupoles, the red elements the dipoles and the black vertical lines the monitor position.

The dispersion (Fig. 3.14) in therapeutic gantries has a high priority, because it influences the beam spot and creates a spatial energy deviation, which hinders the treatment.

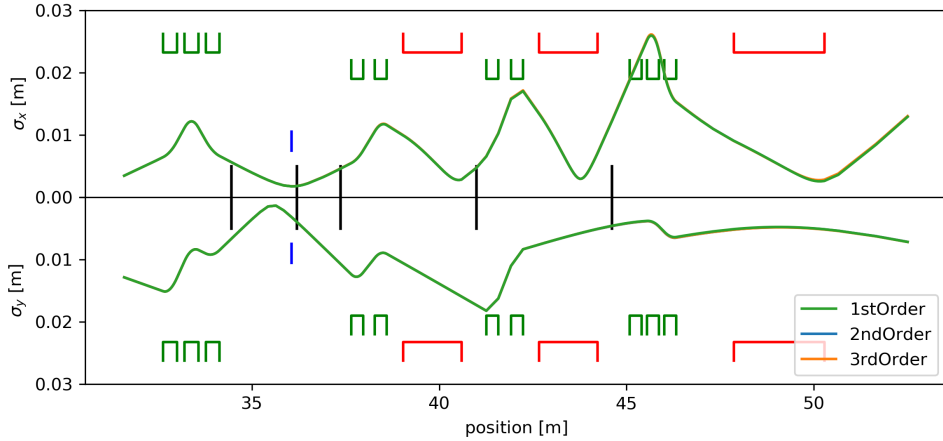


Figure 3.15: PSI gantry 2 envelope plot in different orders; Here, the envelopes were calculated with OPAL-map in the first (green), second (blue) and third order (orange). The green lines indicate the quadrupoles, the red elements the dipoles, the black vertical lines the monitor position and the blue vertical line an aperture.

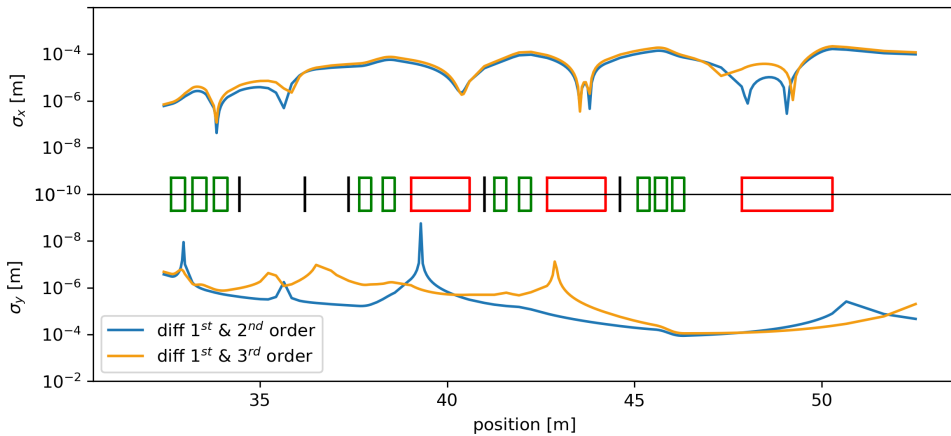


Figure 3.16: PSI gantry 2 difference in envelope plot with OPAL-map in the first three orders; Here, the rms difference in between the first and second (blue) and the first and third order simulation got printed. The green lines indicate the quadrupoles, the red elements the dipoles and the black vertical lines the monitor position.

Considering, that in Fig. 3.16 Gantry 2 is still simplified using no fringe field and no pole face rotation.

Transfermap Gantry2

coefficient	x	px	y	py	z	delta
4.99841426108339e+00	1	0	0	0	0	0
-1.80499976777692e+00	0	1	0	0	0	0
-3.17859777518194e-01	0	0	0	0	0	1
-6.89478372039282e+00	2	0	0	0	0	0
3.99792859086408e+00	1	1	0	0	0	0
-9.36210501042244e+01	1	0	0	0	0	1
-5.562506333915830e-01	0	2	0	0	0	0
-8.18540546639822e+01	0	1	0	0	0	1
-5.19079887330289e-02	0	0	2	0	0	0
-1.43664901906849e-01	0	0	1	1	0	0
-1.73826168418316e-01	0	0	0	2	0	0
6.57053307049404e+01	0	0	0	0	0	2

Figure 3.17: The transfer map of the PSI Gantry 2 for the x coordinate up to the second order

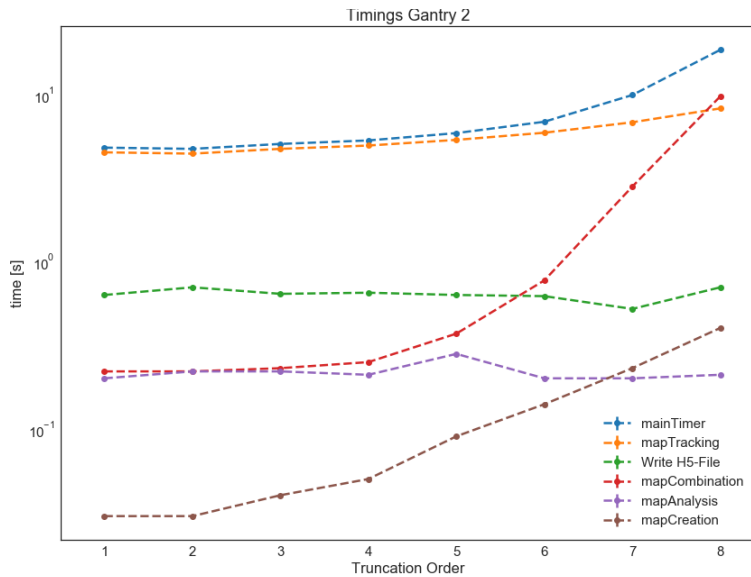


Figure 3.18: PSI gantry 2 simulation timing; #nodes = 1, #particles=1000, #maps=105; The blue line denotes the total simulation time (mainTimer), the orange represents the particle tracking (mapTracking), the green line the creation of the .h5 data files (Write H5-File), the red line the accumulation of the beam line maps (mapCombination), the purple the analysis of the maps (mapAnalysis) and the brown the map creation (mapCreation).

Fig. 3.18 shows the computational times of a Gantry simulation, relative to the truncation order. The processor used for the simulation was a Intel(R) Core(TM) i7-6820HQ CPU @ 2.70GHz.

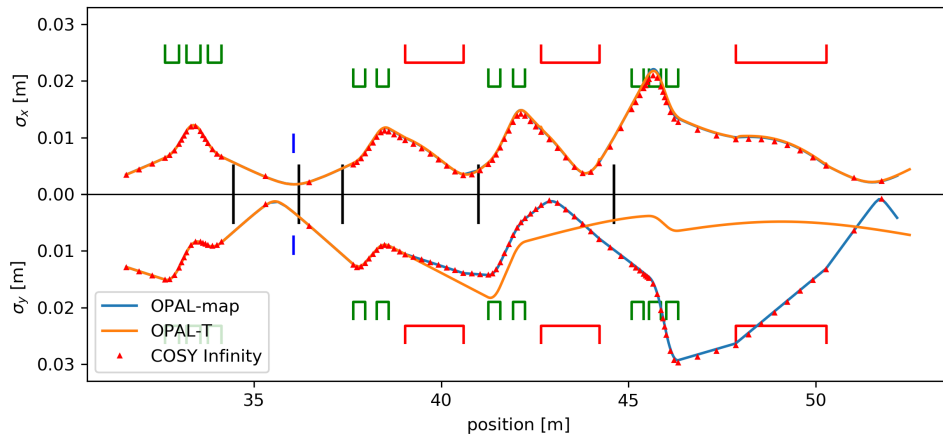


Figure 3.19: PSI gantry 2 envelopes including pole face rotation in 1st order; In this plot the pole face rotation gets implemented, using the map tracking algorithms OPAL-maps (blue line) and COSY Infinity (red triangles) and the particle tracking code OPAL-T (orange line). The green lines indicate the quadrupoles, the red elements the dipoles, the black vertical lines the monitor position and the blue vertical line an aperture.

Chapter 4

Discussion

4.1 Map Comparison

The map comparison showed, that the influence of the different particle mass constants E_0 in the linear case is in the order of magnitude of $1 \cdot 10^{-7}$, whereas the map difference of drift and quadrupole elements is around 10^{-14} and dipoles 10^{-7} . These differences now propagate, as expected, exponentially in higher orders.

These insights open the question about the required map precision.

4.1.1 Map precision

The required precision is dependent on its application. A synchrotron storage ring for example has to full fill the its criteria for a high repetition of the single turn map \mathbf{M}_{ST} of about 10^6 and even more. In a mathematical way, the criteria get tested on accumulated map $\mathbf{M} = \mathbf{M}_{ST}^{10^6}$. Where, on the other hand, a transport beam line, on the other hand, just gets passed once.

In the context of proton therapy, the key factor for its inaccuracy does not come form the beam optics side. Here the problem lies in the treatment planing and its inaccuracies of the of the treatment itself. This error starts in the imaging process and its conversion to stopping power. After the vacuum of the beam line, the beam scatters at the beam nozzle, the air to the patient and in the patient. Additional uncertainties as inter and intra fractional tumor movement or other diverse uncertainties from the patient, as a change of weight, different positioning, and many more, lead to increase of the Planning Target Volume (PTV).

Regardless of those uncertainties, a wrongly adjusted beam line lead to unwanted systematic problems, which could cause repetitive under and over dosage with fatal consequences, especially using the Pencil Beam Scanning (PBS) technique. [4, Chapter 13]

Taking into account upper effects, I suggest that the accuracy of the beam positioning in the order of magnitude 0.1mm would still be sufficient for a successful treatment. This assumption leads to a transfer map precision of the whole beam line in the order of magnitude $1 \cdot 10^{-4}$.

Assuming that the theoretical implementation of the PSI Gantry 2 beam line is correct and the map differences of COSY Infinity and OPAL-map, in the order of magnitude 10^{-7} , is approximately the uncertainty of the map itself, lead to the conclusion, that the OPAL-map algorithm is enough precise for this simulation.

4.2 Envelopes

In all shown examples, the envelope plots show a good match, except in Fig. 3.19. Here a big mismatch occurs in the y plane, between the tdPT and the map tracking *s*-bases algorithms.

4.2.1 Pole Face Rotation

In the non dispersal y plane in OPAL-T no additional effect occurs if a pole face rotation (PFR) gets implemented (Fig. 4.1).

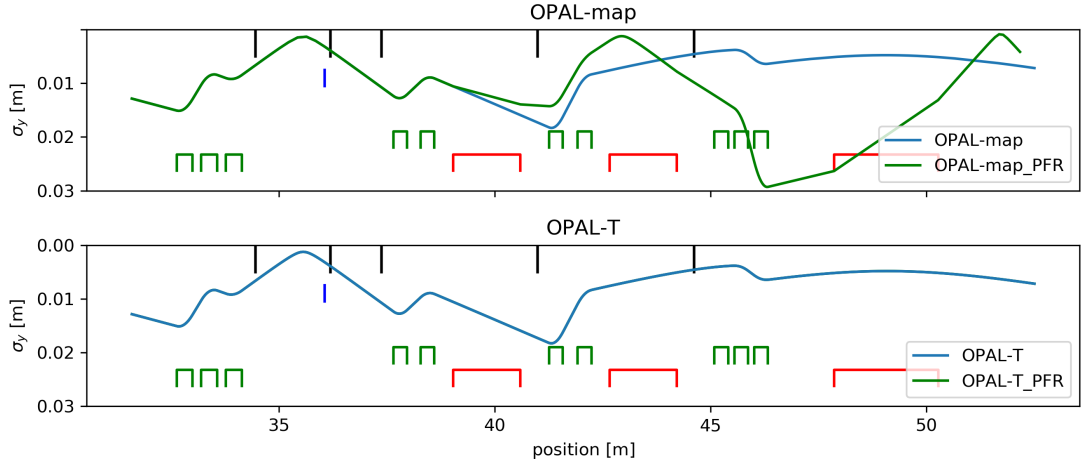


Figure 4.1: PSI gantry 2 envelope comparison in y-plane in- and excluding pole face rotation (PFR); In the upper plot the simulation with OPAL-map and in the lower plot the simulation with OPAL-T is shown. The solid lines represent the envelope including (green) and excluding (blue) the pole face rotation (PFR).

The absence of any effect can be explained with the fringe field implementation with field maps. [1, Section "Field Maps"] In the OPAL-parallelT these field maps define the magnetic field in the transition to and off the element.

The used hard edge model, uses an Enge function (4.1), but with an extreme setting to suppress the size of the fringe field.

$$F(z) = \frac{1}{1 + e^{\sum_{n=0}^N c_n (\frac{z}{D})^n}} \quad (4.1)$$

Where N denotes the edge function order, c_n element dependent fitted parameters and D the aperture of the magnet.

The hard edge model uses $N = 0$ which turns the function into a simple $F = \frac{1}{2}$ and the influence range of the fringe field gets defined with $5 \cdot 10^{-11}$ m. This special implementation not only suppresses any field outside of the magnet, but also leads to a rapid changes of the magnetic field in the tracking algorithm, which leads due to the Maxwell equations in high fields in the x and y plane. This can be seen in small "horns" at the dipole edges (a good example can be seen in Fig. 4.3 in the entrance of AMF3).

The influence range in the hard edge model is approximately zero, which simplifies the system in the way, that only a $B_y(s)$ dependence exists and B_x and B_s are zero. Hence just an effect in the dispersive x plane can be observed.

The default fringe field map in OPAL-T uses proper values for the Enge Model (Fig. 4.2). Here the field outside the magnet gets defined in a realistic way, which leads also to s dependent $B_x(s)$ and $B_s(s)$ components, which lead to an vector potential in s and x as mentioned in 1.2.4 "Dipole - Pole Face Rotation".

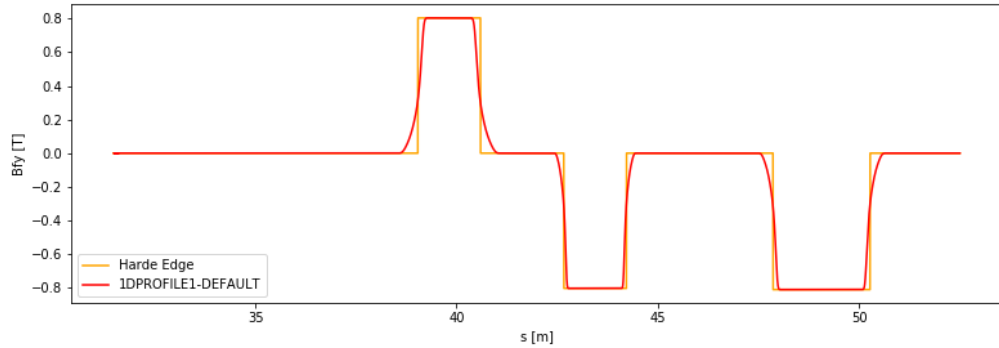


Figure 4.2: PSI gantry 2 magnetic fields in y-axis; In this figure the difference in the magnetic field using the default OPAL field map (1DPROFILE1-DEFAULT, red line) and the hard edge model (orange line) gets illustrated.

Unfortunately, at this moment the A_x effects are not implemented in OPAL-map. Now comparing OPAL-map and OPAL-T using the hard edge or the default field map, leads to Fig. 4.3.

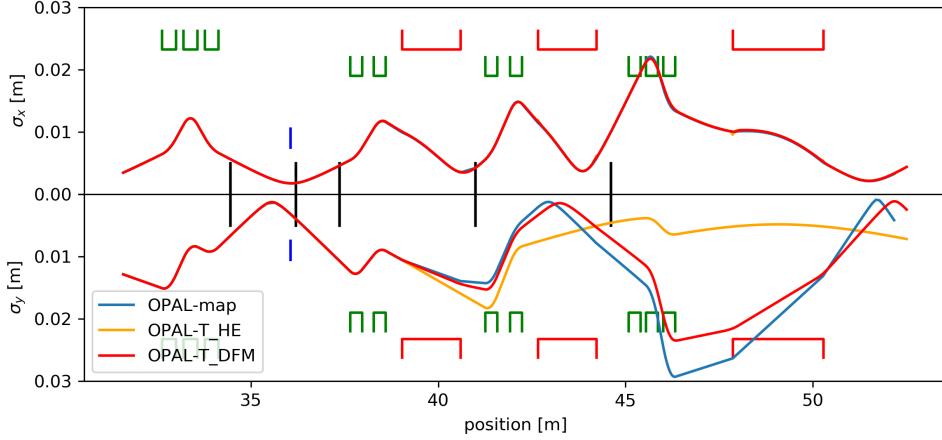


Figure 4.3: PSI Gantry 2 envelopes field map comparison; In this plot, the pole face rotation of the three dipoles (red elements) got implemented. The first order OPAL-map (blue line) envelopes is now used as a reference to compare OPAL-T with the hard edge model (HE, orange line) and the default field map (DFM, red line). The green lines indicate the quadrupoles, the black vertical lines the monitor position and the blue vertical line an aperture.

In this figure a good match can be seen in the x plane. The y plane, on the other hand, shows different envelopes after the dipoles, caused by the effect explained above. It can be seen clearly at the entrance of AMF1. Here, the OPAL-T hard edge can be used as a reference to see the linear effects of OPAL-map and the non-linear on OPAL-T, which uses the default field map.

4.3 Dispersion

The dispersion of OPAL-map, OPAL-T and the analytical solution of pyAcceLEGOrator (pyAcceL) show a good match.

The dispersion is an important property for therapeutic gantries. In many cases it is the goal to reach a completely achromatic behavior $\Sigma_{1,6} = \Sigma_{2,6} = 0$. Dispersion at the isocenter would cause many difficulties for a precise dose delivery, because it not only increases the beam spread $\eta_{px} = \Sigma_{2,6}$ but also results in a spatial energy deviation $\eta_x = \Sigma_{1,6}$. In proton therapy the particle energy is related to the debt of the Bragg Peak, which forms the basic principle of particle therapy. These two effects would now lead to a widening of the focal spot in along the dispersal axis and rotation of the focal plane along the y axis.

In the comparison of the dispersion of OPAL-map and OPAL-T 3.14 shows slight differences. This is because OPAL-T has no possibility to gain the information for the dispersion out of the beam line, so the information gets attained out of the Sigma Matrix (Σ) $\eta_x = \Sigma_{1,6}$ and $\eta_{px} = \Sigma_{2,6}$ and scaled with the beam emittance in the z- and x-plane. This procedure not only is computationally more expensive, but also bears statistical influences and a dependency in the initial Σ . These artificial effects can be seen at the first quadrupole triplet.

4.4 Complexity

To understand the timings Fig. 3.18 is important to understand the mathematical operations, focusing on the two biggest components the "mapTracking" and "mapCombination". For further explanations, the data types for the map gets denoted, as previously with \mathcal{M} and its elements \mathcal{S} , a truncated power series. In ${}_n D_\nu \mathcal{M}$ is an vector with the size of the dimension ν , in our case $\nu = 6$, containing the data \mathcal{S} , which is a polynomial of order n .

$$\mathcal{M} = \begin{pmatrix} \mathcal{S}_x \\ \mathcal{S}_{p_x} \\ \mathcal{S}_y \\ \mathcal{S}_{p_y} \\ \mathcal{S}_z \\ \mathcal{S}_\delta \end{pmatrix} \quad \mathcal{S}_x = k_x x + k_{p_x} p_x + \dots + k_{xy\delta} xy\delta + \dots \quad (4.2)$$

Where k_i is the coefficient of the monomial i .

4.4.1 Accumulation of element maps

- "mapCombination"

This procedure describes the application of one map on an other $\mathcal{M}_2 \circ \mathcal{M}_1$. In this operation all the terms of the polynomial of each dimension \mathcal{S}'_i of the left hand side get multiplied, according to its monomial, with the contained series \mathcal{S}_i of the right hand side.

$$\mathcal{M} = \mathcal{M}_2 \circ \mathcal{M}_1 = \begin{pmatrix} \mathcal{S}'_x \\ \mathcal{S}'_{p_x} \\ \mathcal{S}'_y \\ \mathcal{S}'_{p_y} \\ \mathcal{S}'_z \\ \mathcal{S}'_\delta \end{pmatrix} \circ \begin{pmatrix} \mathcal{S}_x \\ \mathcal{S}_{p_x} \\ \mathcal{S}_y \\ \mathcal{S}_{p_y} \\ \mathcal{S}_z \\ \mathcal{S}_\delta \end{pmatrix} \quad (4.3)$$

$$\mathcal{S}'_x = k' x_x \cdot x + k' x_{p_x} \cdot p_x + k' x_y \cdot y + k' x_{p_y} \cdot p_y + \dots \quad (4.4)$$

$$\mathcal{M} = \begin{pmatrix} k' x_x \cdot \mathcal{S}_x + k' x_{p_x} \cdot \mathcal{S}_{p_x} + k' x_y \cdot \mathcal{S}_y + \dots \\ k' p_{x,x} \cdot \mathcal{S}_x + k' p_{x,p_x} \cdot \mathcal{S}_{p_x} + k' p_{x,y} \cdot \mathcal{S}_y + \dots \\ \dots \\ k' \delta_x \cdot \mathcal{S}_x + k' \delta_{p_x} \cdot \mathcal{S}_{p_x} + k' \delta_y \cdot \mathcal{S}_y + \dots \end{pmatrix} \quad (4.5)$$

Assuming a full map and the full extend of the mathematical operation leads to a scaling according to (4.6), visualized in Fig. 3.18.

$$T = \nu \sum_{j=1}^n K \cdot P^N \quad (4.6)$$

$$K = \binom{n+\nu-1}{\nu-1} = \frac{(n+\nu-1)!}{n! (\nu-1)!}, \quad P = \sum_{j=0}^n K \quad (4.7)$$

In this formula T denotes the total numbers of Multiplications, where K and P represent the number of monomials with the order n and the total number, in the dimension ν .

Considering that the truncation order O of the map will rise according to $O(M_1 \circ M_2) = O(M_1) + O(M_2)$. Thus, this process would rise the order n of the map \mathcal{M} , creating non wanted therm. In the OPAL-DA package, the number of multiplications is decreased drastically, by neglecting all the calculations, which would result in a order higher as the truncation order and also neglecting the constant therm.

4.4.2 Tracking through maps

- "mapTracking"

This process describes the application of the transfer map \mathcal{M} on the bunch. For one particle, the polynomial in each dimension S_i get evaluated using the particle properties. For one particle, this process scales with the size of the ${}_nD_\nu$ times the dimension (4.8) (Fig. 4.4).

$$T = \nu \cdot P \quad (4.8)$$

Where ν is the dimension and P ((4.7)) the number of possible polynomials in of the ${}_nD_\nu$.

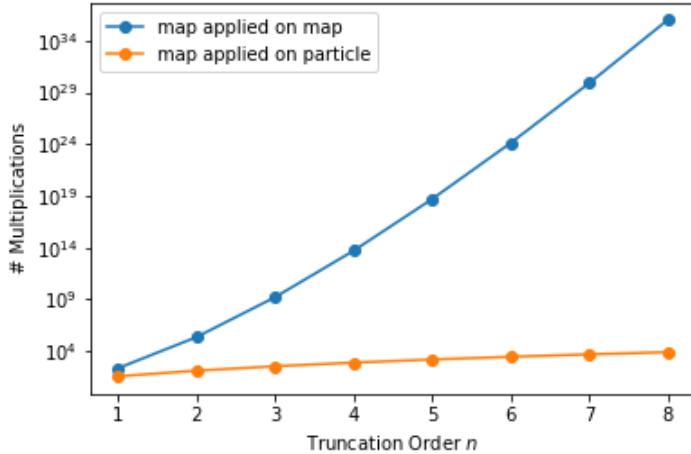


Figure 4.4: Number of multiplications in ${}_nD_6$ in order n ; This figure illustrates the effect of the complexity in calculations in ${}_nD_6$, if a full map gets applied on an other map (blue) or used to track a particle (orange).

Chapter 5

Conclusion

OPAL-map is a map tracking program, which creates maps with Lie series calculating these with Truncated Power Series Algebra (TPSA). This procedure allows to generate higher order maps from the pre-defined element Hamiltonians. [2]

For a reference the output was compared with other beam optics programs: COSY Infinity [12], pyAcceL [13] and OPAL-T [1]. Where each of those programs brings a different calculation approach: COSY Infinity uses similar mathematics for the map creation, pyAcceL the first order analytical solution for the maps and OPAL-T tdPT.

The differences in between the maps of COSY Infinity and OPAL-map were analyzed. It was seen, that the linear coefficient in a drift or quadrupole map differ the order of magnitude 10^{-14} and the one of dipole maps in 10^{-7} .

For proton therapy we assumed an spatial precision of 0.1mm, which would lead to a map precision of $1 \cdot 10^{-4}$. Hence OPAL-map can be used for the simulation of PSI Gantry 2. For repetitive beam lines as synchrotrons the precision criteria would increase, but could also change to a symplecticity criteria [10].

The envelopes of all codes match, except in between OPAL-map and OPAL-T in 4.3. This can be explained due to the absence of higher order fringe field effects, which is currently not implemented in OPAL-map. This plot also points out the focusing effect of the pole face rotated dipoles in PSI Gantry 2.

An other advantage of OPAL-map can be seen in the calculation of the dispersion (Fig. 3.14). Where tdPT programs, as OPAL-T, need to extract the data form Σ , MT program can calculate it from their maps. Latter procedure is computationally less expensive and does not contain statistical or artificial, due to a coupled beam, errors.

Unfortunately, OPAL-map can only analyze the PSI Gantry 2 in the first order which is not sufficient enough, due to the higher order form the fringe fields at the bending magnets, which is currently not implemented.

On the other hand, OPAL-map can provide due to its map analysis the dispersion and the complete 1st order transfer map which can be used as a fast simulation for optimize programs, as OPAL opt-pilot.

5.1 Outlook

OPAL-map is a map tracking code in its early stages which potentials is not sufficiently explored. The current stand of the program forms a solid foundation, but there are many possibilities, in which it can develop.

In my opinion, the non linear fringe fields should get addressed first to provide widen the practicability. In a second step the performance should get improved in parallelize the particle tracking and even make it optional.

Furthermore, the implementation of space charge effects could lead to a bigger applicability especially in the field high intensity beams.

I would also suggest to implement an lateral offset to the beam line elements, this would provide the possibility to simulate Fixed-Field Alternating Gradient (FFAG) lattices, which also gets, in conceptional studies, applied on gantries [15].

Chapter 6

Acknowledgement

Last but not least, I want to take this opportunity to thank of my supervisor Prof. Dr. Antony John Lomax. He not only gave me the chance to work on the project, but also gave the freedom to guide its scope in my preferred direction.

Second, but at least as grateful, I want to thank my supervisor Dr. Andreas Adelmann for his great support. His advices were always as friendly as competent and there was no time, he refused to help, even in unorthodox situations.

Special thanks belong to Matthias Frey, who did't just once helped me, at the brink of despair, in programming issues.

I also want to mention Valeria Rizzoglio, her simulation skills and good timed inputs were from great importance for the project. Grazie mille.

During my thesis Prof. Dr. Peter Arbenz provided me an office to whom and his group I want to convey my gratefulness for sharing the facility and the warm atmosphere.

At the end, I also want to thank Marija Kranjčević who always took care of a nice environment and being accommodative independent the problem kind.

Chapter 7

Acronyms

DA	Differential Algebra	iii
FSC	Frenet-Serret Coordinates.....	2
MT	Map Tracking	1
PBS	Pencil Beam Scanning.....	34
PSI	Paul Scherrer Institute	27
tdPT	time dependent Particle Tracking ..	5
pyAcceL	pyAcceLEGOrator	37
RF	Radio Frequency	27
RP	Reference Particle	2
Σ	Sigma Matrix.....	3
TPSA	Truncated Power Series Algebra ...	1

Appendix A

Units

quantity	symbol	SI unit	C, N unit	e, V unit
charge	q	A s	C	e
charge density	ρ	A s m^{-3}	C m^{-3}	e m^{-3}
current	I	A	Cs^{-1}	e s^{-1}
electric field	\vec{E}	$\text{kg m A}^{-1} \text{s}^{-3}$	N C^{-1}	V m^{-1}
mass	m	kg	kg	MeV c^{-2}
potential	ϕ	$\text{kg m}^2 \text{A}^{-1} \text{s}^{-3}$	N m C^{-1}	V
speed of light	c	m s^{-1}	m s^{-1}	1
vacuum permittivity	ϵ_0	$\text{A}^2 \text{s}^4 \text{kg}^{-1} \text{m}^{-3}$	$\text{C}^2 \text{N}^{-1} \text{m}^{-2}$	$\text{e V}^{-1} \text{m}^{-1}$

Table A.1: Symbols and their corresponding units.

Appendix B

complete transfer matrix FODO

```

Transfermap FODO
FVps 6
Tps 1 5 5 6
 0.0000000000000e+00 -1 -1 -1 -1 -1 -1
-1.02619697697268e+00 1 0 0 0 0 0 0
-1.99970538528579e-01 0 1 0 0 0 0 0
-7.43993992258748e-01 1 0 0 0 0 0 1
6.81372414922869e+00 0 1 0 0 0 0 1
4.24058384937832e-01 3 0 0 0 0 0 0
-2.01179574465487e+00 2 1 0 0 0 0 0
1.21249388325331e-01 1 2 0 0 0 0 0
1.52926590368216e+00 1 0 2 0 0 0 0
3.42916108688955e+00 1 0 1 1 0 0 0
1.76109899012140e+00 1 0 0 2 0 0 0
2.60280764146783e+01 1 0 0 0 0 0 2
-1.33623600329734e+00 0 3 0 0 0 0 0
-2.77504233826512e+00 0 1 2 0 0 0 0
-5.85149886953810e+00 0 1 1 1 0 0 0
-3.92870468155939e+00 0 1 0 2 0 0 0
-1.8433935834320e+01 0 1 0 0 0 0 2
-2.23431763165446e+01 3 0 0 0 0 0 1
8.34290748370170e+00 2 1 0 0 0 0 1
-8.76076780234036e+00 1 2 0 0 0 0 1
-4.96248117644509e+01 1 0 2 0 0 0 1
-1.32620538951324e+02 1 0 1 1 0 0 1
-9.05182976745489e+01 1 0 0 2 0 0 1
-1.87516900012715e+02 1 0 0 0 0 0 3
7.60422966713986e+00 0 3 0 0 0 0 1
3.65360097532672e+01 0 1 2 0 0 0 1
9.16576791159192e+01 0 1 1 1 0 0 1
5.83021391835188e+01 0 1 0 2 0 0 1
-1.43197780979596e+01 0 1 0 0 0 0 3
4.69597202154060e+00 5 0 0 0 0 0 0
-2.95863471701198e+00 4 1 0 0 0 0 0
5.13933937882824e+00 3 2 0 0 0 0 0
2.000861036366888e+01 3 0 2 0 0 0 0
5.05260940540323e+01 3 0 1 1 0 0 0
3.36113373648445e+01 3 0 0 2 0 0 0
2.77468301425413e+02 3 0 0 0 0 0 2
-2.31192252348781e+00 2 3 0 0 0 0 0
-1.72184066285795e+01 2 1 2 0 0 0 0
-4.45968553991475e+01 2 1 1 1 0 0 0
-2.79438133490200e+01 2 1 0 2 0 0 0
6.65567294395602e+01 2 1 0 0 0 0 2
1.91392531523853e+00 1 4 0 0 0 0 0
1.53477262508380e+01 1 2 2 0 0 0 0
3.61071320478062e+01 1 2 1 1 0 0 0
2.07499053985411e+01 1 2 0 2 0 0 0
1.21586965879912e+02 1 2 0 0 0 0 2
2.23751904278160e+01 1 0 4 0 0 0 0
1.15059523710264e+02 1 0 3 1 0 0 0
2.241884506363375e+02 1 0 2 2 0 0 0
6.88810786835147e+02 1 0 2 0 0 0 2
1.97855906338854e+02 1 0 1 3 0 0 0
2.02373663075744e+03 1 0 1 1 0 0 2
6.70211227781389e+01 1 0 0 4 0 0 0
1.4935899460323e+03 1 0 0 2 0 0 2
1.08870206152438e+03 1 0 0 0 0 0 4
-7.798322502561185e-01 0 5 0 0 0 0 0
-5.89944727787898e+00 0 3 2 0 0 0 0
-1.35714830807599e+01 0 3 1 1 0 0 0
-7.88592510504037e+00 0 3 0 2 0 0 0
2.07532826759046e+01 0 3 0 0 0 0 2
-2.77198240248643e+01 0 1 4 0 0 0 0
-1.33338627318518e+02 0 1 3 1 0 0 0
-2.461713210226608e+02 0 1 2 2 0 0 0
-2.60486024074888e+02 0 1 2 0 0 0 2
-2.08072336009831e+02 0 1 1 3 0 0 0
-8.03504748671027e+02 0 1 1 1 0 0 2
-6.78794591587843e+01 0 1 0 4 0 0 0
-5.50006895117139e+02 0 1 0 2 0 0 2
5.75845040597092e+02 0 1 0 0 0 4 0
0.0000000000000e+00 -1 -1 -1 -1 -1 -1

```

```

Tp 1 5 5 6
-1.28079421796587e+00 0 0 1 0 0 0
-1.99974861517258e-01 0 0 0 1 0 0
2.20262403512728e+01 0 0 1 0 0 1
3.17320919492645e+01 0 0 0 1 0 1
-8.02503860781498e+00 2 0 1 0 0 0
-1.15802928338253e+01 2 0 0 1 0 0
5.56304146780108e-01 1 1 1 0 0 0
-7.85395019290712e-01 1 1 0 1 0 0
-3.05664711790012e+00 0 2 1 0 0 0
-4.40979065053272e+00 0 2 0 1 0 0
-1.94318801717064e+01 0 0 3 0 0 0
-7.54045534872191e+01 0 0 2 1 0 0
-1.02146764013813e+02 0 0 1 2 0 0
-1.26299613861916e+02 0 0 1 0 0 2
-4.87234723483412e+01 0 0 0 3 0 0
-4.45590713951376e+02 0 0 0 1 0 2
1.12337894646518e+02 2 0 1 0 0 1
1.84825482226174e+02 2 0 0 1 0 1
2.49321713894786e+01 1 1 1 0 0 1
5.67116253244367e+01 1 1 0 1 0 1
2.98657246103965e+01 0 2 1 0 0 1
6.90216297565713e+01 0 2 0 1 0 1
2.97703598663921e+02 0 0 3 0 0 1
1.31190732334140e+03 0 0 2 1 0 1
1.94656391416748e+03 0 0 1 2 0 1
6.57499937603824e+02 0 0 1 0 0 3
1.00044455638800e+03 0 0 0 3 0 1
1.51300977228955e+03 0 0 0 1 0 3
-2.98788391217554e+01 4 0 1 0 0 0
-4.22419344056241e+01 4 0 0 1 0 0
-6.4994967475585e+00 3 1 1 0 0 0
-1.64028426513492e+01 3 1 0 1 0 0
-2.24776335048579e+01 2 2 1 0 0 0
-3.72602645048830e+01 2 2 0 1 0 0
-1.30256655303793e+02 2 0 3 0 0 0
-5.29591677106526e+02 2 0 2 1 0 0
-7.30313425261920e+02 2 0 1 2 0 0
-1.07483011639000e+03 2 0 1 0 0 2
-3.47554876209746e+02 2 0 0 3 0 0
-1.90569371766442e+03 2 0 0 1 0 2
-1.32654698042186e+00 1 3 1 0 0 0
-7.02302932945228e+00 1 3 0 1 0 0
2.88803533677383e+00 1 1 3 0 0 0
-2.433363385805821e+01 1 1 2 1 0 0
-8.572144137779894e+01 1 1 1 2 0 0
-4.846130083836258e+02 1 1 1 0 0 2
-6.72791434850101e+01 1 1 0 3 0 0
-9.42571723639016e+02 1 1 0 1 0 2
-1.75660549739085e+00 0 4 1 0 0 0
-5.19446299334552e+00 0 4 0 1 0 0
-3.82231936919193e+01 0 2 3 0 0 0
-1.72614880528381e+02 0 2 2 1 0 0
-2.61937155210405e+02 0 2 1 2 0 0
-2.247001653729300e+02 0 2 1 0 0 2
-1.39112539944064e+02 0 2 0 3 0 0
-6.74836549429177e+02 0 2 0 1 0 2
-1.60959042510642e+02 0 0 5 0 0 0
-1.05164713860096e+03 0 0 4 1 0 0
-2.80616845470111e+03 0 0 3 2 0 0
-3.09046775932426e+03 0 0 3 0 0 2
-3.84623894625317e+03 0 0 2 3 0 0
-1.49347321949504e+04 0 0 2 1 0 2
-2.72024746830315e+03 0 0 1 4 0 0
-2.38419285722741e+04 0 0 1 2 0 2
-3.28513079126854e+03 0 0 1 0 0 4
-7.98677528904790e+02 0 0 0 5 0 0
-1.29263276613380e+04 0 0 0 3 0 2
-8.50918565654172e+03 0 0 0 1 0 4
0.00000000000000e+00 -1 -1 -1 -1 -1 -1

Tp 1 5 5 6
-3.28626015289046e-15 0 0 0 0 0 0
1.00000000000000e+00 0 0 0 0 1 0
1.64798308373764e+01 0 0 0 0 0 1
-3.06982988449752e+00 2 0 0 0 0 0
-4.71407623472574e+01 1 1 0 0 0 0
-3.36582154331609e+00 0 2 0 0 0 0
-8.66263395824743e+00 0 0 2 0 0 0
-1.99023840411362e+01 0 0 1 1 0 0
-1.39413763510236e+01 0 0 0 2 0 0
-5.77300464737216e+01 0 0 0 0 0 2
2.5304598445865e+01 2 0 0 0 0 1
2.42515392648601e-01 1 1 0 0 0 1
2.1992257315348e+01 0 2 0 0 0 1
1.18093458913515e+02 0 0 2 0 0 1
3.21068730837990e+02 0 0 1 1 0 1
2.23603121636431e+02 0 0 0 2 0 1
2.16462921423769e+02 0 0 0 0 0 3
-7.87741190064133e+00 4 0 0 0 0 0
3.0118072207227041e+00 3 1 0 0 0 0
-6.16970970212789e+00 2 2 0 0 0 0
-4.82848084795359e+01 2 0 2 0 0 0
-1.26548059479708e+02 2 0 1 1 0 0
-8.22736236061913e+01 2 0 0 2 0 0
-2.24010599565659e+02 2 0 0 0 0 2
2.86614366162964e+00 1 3 0 0 0 0
1.08108581731976e+01 1 1 2 0 0 0
1.96928708303105e+01 1 1 1 1 0 0
6.96579403342028e+00 1 1 0 2 0 0
2.43050405340039e+00 1 1 0 0 0 2
-2.37211488557621e+00 0 4 0 0 0 0
-1.79768966128738e+01 0 2 2 0 0 0
-4.6259188127577e+01 0 2 1 1 0 0
-3.1105909060209e+01 0 2 0 2 0 0
-8.51848492774929e+01 0 2 0 0 0 2
-7.85750731862969e+01 0 0 4 0 0 0
-3.95643277355737e+02 0 0 3 1 0 0
-7.66138002987570e+02 0 0 2 2 0 0
-1.15324540761758e+03 0 0 2 0 0 2
-6.80154362389132e+02 0 0 1 3 0 0
-3.5897799678807e+03 0 0 1 1 0 2
-2.33734882854660e+02 0 0 0 4 0 0
-2.71747993719382e+03 0 0 0 2 0 2
-8.46179559533420e+02 0 0 0 0 0 4
1.732699980969561e+02 4 0 0 0 0 1
-1.84555478916454e+01 3 1 0 0 0 1
9.07892060685083e+01 2 2 0 0 0 1
1.07615355834090e+03 2 0 2 0 0 1
3.11261658139000e+03 2 0 1 1 0 1
2.22308710859384e+03 2 0 0 2 0 1
1.89484170304707e+03 2 0 0 0 0 3
-2.58889348276695e+01 1 3 0 0 0 1
-5.754121811176510e+01 1 1 2 0 0 1
-3.65919024225999e+00 1 1 1 1 0 1

```

```

1.12301510386757e+02  1  1  0  2  0  1
3.83570267118253e+02  1  1  0  0  0  3
4.11235711821529e+00  0  4  0  0  0  1
2.99915510004025e+02  0  2  2  0  0  1
9.67492771415452e+02  0  2  1  1  0  1
7.34510080050207e+02  0  2  0  2  0  1
1.40500997129049e+02  0  2  0  0  0  3
1.82713998389005e+03  0  0  4  0  0  1
1.01094375948748e+04  0  0  3  1  0  1
2.11806481529668e+04  0  0  2  2  0  1
9.37833750178960e+03  0  0  2  0  0  3
2.01155238172603e+04  0  0  1  3  0  1
3.24749662621335e+04  0  0  1  1  0  3
7.33392347319989e+03  0  0  0  4  0  1
2.68893828307430e+04  0  0  0  2  0  3
3.39472708565487e+03  0  0  0  0  0  5
0.00000000000000e+00 -1 -1 -1 -1 -1 -1

```

Tps 1 1 5 6
1.00000000000000e+00 0 0 0 0 0 1
0.00000000000000e+00 -1 -1 -1 -1 -1 -1

Appendix C

Canonical Transformations

C.1 Canonical transformation of the independent variable $t \rightarrow s$

As mentioned in section 1.2.3, the bunch position s provides an easy handling of the application of the maps. The change independent variable can be done using the action S considering the principle of Least Action:

$$\delta S = \delta \left[\int_{t_0}^{t_1} L dt \right] = 0 \quad (\text{C.1})$$

$$S = \int_{t_0}^{t_1} (p_x \dot{x} + p_y \dot{y} + p_z \dot{z} - H) dt \quad (\text{C.2a})$$

$$= \int_{z_0}^{z_1} \left(p_x \frac{dx}{dz} + p_y \frac{dy}{dz} + p_z - H \frac{dt}{dz} \right) dz \quad |(\cdot)' := \frac{d \cdot}{dz} \quad (\text{C.2b})$$

$$= \int_{z_0}^{z_1} (p_x x' + p_y y' + p_z - H t') dz \quad (\text{C.2c})$$

$$= \int_{z_0}^{z_1} (p_x x' + p_y y' - H t' + p_z) dz \quad (\text{C.2d})$$

Using equation (C.2d) the Hamiltonian H can be redefined.

$$(x, p_x) \quad (y, p_y) \quad (-t, H) \quad (\text{C.3})$$

$$H_1 = p_z \quad (\text{C.4})$$

Rearranging equation (1.27) leads to:

$$p_z = H_1 = \sqrt{\frac{(E - q\Phi)^2}{c^2} - (mc)^2 - (p_x - A_x q)^2 - (p_y - A_y q)^2 + A_z q} \quad (\text{C.5})$$

To keep the values low, it is a good approach to normalize the momenta design momentum P_0 .

Therefore the whole equation (C.5) receives above normalization.

$$\tilde{p}_i := \frac{p_i}{P_0} \quad i = x, y, z \quad (\text{C.6a})$$

$$\tilde{H}_1 := \frac{H_1}{P_0} \quad (\text{C.6b})$$

$$\tilde{a}_i := q \frac{A_i}{P_0} \quad i = x, y, z \quad (\text{C.6c})$$

Including those normalizations results in

$$H_1 = \sqrt{\frac{(E - q\Phi)^2}{c^2} - (mc)^2 - (p_x - A_x q)^2 - (p_y - A_y q)^2 + A_z q} \quad | \frac{\circ}{P_0} \quad (\text{C.7})$$

$$\tilde{H}_1 = \sqrt{\frac{(E - q\Phi)^2}{(P_0 c)^2} - \left(\frac{mc}{P_0}\right)^2 - (\tilde{p}_x - a_x)^2 - (\tilde{p}_y - a_y)^2 + a_z} \quad (\text{C.8})$$

C.2 Canonical transformation of the dependent variable $E \rightarrow \delta$

The normalized transverse momenta \tilde{p}_x and \tilde{p}_y now contain small values, but the normalized longitudinal momentum $\frac{E}{P_0}$ is still in order of magnitude of the speed of light c . For a smaller value, a canonical transformation 2nd kind is used.

$$F_2(x, P_x, P_y, -t, \delta : z) = xP_x + yP_0 + \left(\frac{z}{\beta_0} - ct\right) \left(\frac{1}{\beta_0} + \delta\right) \quad (\text{C.9})$$

The new momenta are parametrized with P_x , P_y and δ .

$$\tilde{p}_i = \frac{\partial F_2}{\partial q_i} \quad Q_i = \frac{\partial F_2}{\partial P_i} \quad K = \tilde{H} + \frac{\partial F_2}{\partial z} \quad (\text{C.10})$$

$$P_x = \tilde{p}_x \quad X = x \quad (\text{C.11})$$

$$P_y = \tilde{p}_y \quad Y = y \quad (\text{C.12})$$

$$c \left(\frac{1}{\beta_0} + \delta\right) = \frac{E}{P_0} \quad Z = \frac{y}{\beta_0} - ct \quad (\text{C.13})$$

The normalized longitudinal momentum is

$$\delta = \frac{E}{P_0 c} - \frac{1}{\beta_0} = \frac{1}{\beta_0} \frac{E - E_0}{E_0} \quad (\text{C.14})$$

The transformed Hamiltonian K , neglecting the constant therm:

$$K = \frac{\delta}{\beta_0} - \sqrt{\left(\frac{1}{\beta_0} + \delta - \frac{q\Phi}{P_0 c}\right)^2 - (P_x - a_x)^2 - (P_y - a_y)^2 - \left(\frac{mc}{P_0}\right)^2 - a_z} \quad (\text{C.15})$$

Considering relativistic relations simplifies (C.15)

$$E_0 = m_0 c^2, \quad P_0 = \gamma_0 m_0 v = \gamma_0 \beta_0 c \frac{E_0}{c^2} \quad (\text{C.16})$$

$$\frac{mc}{P_0} = \frac{\frac{E_0}{c}}{\frac{\beta_0 \gamma_0 E_0}{c}} = \frac{1}{\beta_0 \gamma_0} \quad (\text{C.17})$$

Renaming the some parameters delivers the basic general Hamiltonian for a straight trajectory (1.28).

$$K \rightarrow H, \quad P_i \rightarrow p_i, \quad z \rightarrow s, \quad Z \rightarrow z \quad (\text{C.18})$$

$$H = \frac{\delta}{\beta_0} - \sqrt{\left(\frac{1}{\beta_0} + \delta - \frac{q\Phi}{P_0 c}\right)^2 - (p_x - a_x)^2 - (p_y - a_y)^2 - \frac{1}{(\beta_0 \gamma_0)^2} + a_s} \quad (\text{C.19})$$

C.3 Canonical transformation for curved trajectories

In the following deviation, the lower case letters as x, y, z represent the Cartesian, whereas X, Y, S represent the new FSC parameters.

$$x = (\rho + X) \cos\left(\frac{S}{\rho}\right) - \rho \quad (\text{C.20a})$$

$$y = Y \quad (\text{C.20b})$$

$$z = (\rho + X) \sin\left(\frac{S}{\rho}\right) \quad (\text{C.20c})$$

Using the third type of generating Functions:

$$x_i = -\frac{\partial F_3}{\partial p_i} \quad P_i = -\frac{\partial F_3}{\partial X_i} \quad (\text{C.21})$$

$$F_3(X, p_x, Y, p_y, S, p_z) = -\left[(\rho + X) \cos\left(\frac{S}{\rho}\right) - \rho \right] p_x - Y p_y - \left[(\rho + X) \sin\left(\frac{S}{\rho}\right) \right] p_z \quad (\text{C.22})$$

The transverse momenta

$$P_X = p_x \cos\left(\frac{S}{\rho}\right) + p_z \sin\left(\frac{S}{\rho}\right) \quad (\text{C.23a})$$

$$P_Y = p_y \quad (\text{C.23b})$$

$$P_S = p_z \left(1 + \frac{X}{\rho}\right) \cos\left(\frac{S}{\rho}\right) - p_x \left(1 + \frac{X}{\rho}\right) \sin\left(\frac{S}{\rho}\right) \quad (\text{C.23c})$$

Considering the curved trajectory, the vector potential also has to be transformed, which results are in the equations below.

$$A_X = A_x \cos\left(\frac{S}{\rho}\right) - A_y \sin\left(\frac{S}{\rho}\right) \quad (\text{C.24a})$$

$$A_Y = A_y \quad (\text{C.24b})$$

$$A_S = A_z \cos\left(\frac{S}{\rho}\right) + A_x \sin\left(\frac{S}{\rho}\right) \quad (\text{C.24c})$$

The Hamiltonian for a curved trajectory can now be formed.

$$H = \frac{\delta}{\beta_0} - (1 + hx) \sqrt{\left(\frac{1}{\beta_0} + \delta - \frac{q\Phi}{P_0 c}\right)^2 - (p_x - a_x)^2 - (p_y - a_y)^2 - \frac{1}{(\beta_0 \gamma_0)^2} + (1 + hx) a_s} \quad (\text{C.25})$$

Appendix D

Complete Transfer Map PSI Gantry 2

```

Gantry2
FVps 6
Tps 0 2 2 6
-5.89816075390077e-16 0 0 0 0 0 0
4.99841426108339e+00 1 0 0 0 0 0
-1.80499976777692e+00 0 1 0 0 0 0
-3.17859777518194e-01 0 0 0 0 0 1
-6.89478372039282e+00 2 0 0 0 0 0
3.99792859086408e+00 1 1 0 0 0 0
-9.36210501042244e+01 1 0 0 0 0 1
-5.56250633915830e-01 0 2 0 0 0 0
-8.18540546639522e+00 0 1 0 0 0 1
-5.19079887330289e-02 0 0 2 0 0 0
-1.43664901906849e-01 0 0 1 1 0 0
-1.73826168418316e-01 0 0 0 2 0 0
6.57053307049404e+01 0 0 0 0 0 2
0.000000000000000e+00 -1 -1 -1 -1 -1 -1
Tps 0 2 2 6
4.42233699501565e-17 0 0 0 0 0 0
1.87772176618226e+00 1 0 0 0 0 0
-4.78009069898658e-01 0 1 0 0 0 0
-8.53317191781775e-01 0 0 0 0 0 1
3.47470032861851e+00 2 0 0 0 0 0
-2.32637927492390e+00 1 1 0 0 0 0
2.94077348273114e+01 1 0 0 0 0 1
4.02246804955143e-01 0 2 0 0 0 0
-5.03223207545248e+01 0 1 0 0 0 1
-8.75903146620293e-04 0 0 2 0 0 0
-1.19484184366316e-01 0 0 1 1 0 0
1.37306526332084e-01 0 0 0 2 0 0
1.01058818554427e+02 0 0 0 0 0 2
0.000000000000000e+00 -1 -1 -1 -1 -1 -1
Tps 1 2 2 6
1.14197648118929e+00 0 0 1 0 0 0
-3.66784233054528e+00 0 0 0 1 0 0
-3.08921935431020e-01 1 0 1 0 0 0
-1.11188305532118e+00 1 0 0 1 0 0
2.55309887510258e-03 0 1 1 0 0 0
2.16668246999105e-01 0 1 0 1 0 0
-9.02297841098092e+00 0 0 1 0 0 1
-1.08828372774235e+02 0 0 0 1 0 1
0.000000000000000e+00 -1 -1 -1 -1 -1 -1
Tps 1 2 2 6
-7.57546504985284e-02 0 0 1 0 0 0
1.11898636695509e+00 0 0 0 1 0 0
1.835270197644464e-01 1 0 1 0 0 0
-2.12997753910986e-01 1 0 0 1 0 0
-4.08558133710974e-02 0 1 1 0 0 0
1.14347513912985e-01 0 1 0 1 0 0
9.23879618663931e+00 0 0 1 0 0 1
-1.36128920495746e+01 0 0 0 1 0 1
0.000000000000000e+00 -1 -1 -1 -1 -1 -1
Tps 0 2 2 6
-4.73773806638681e-14 0 0 0 0 0 0
3.66838059778988e+00 1 0 0 0 0 0
-1.38629747639648e+00 0 1 0 0 0 0
1.000000000000000e+00 0 0 0 0 1 0
1.29942210732428e+02 0 0 0 0 0 1
-1.68381067305892e+02 2 0 0 0 0 0
1.01983629214248e+02 1 1 0 0 0 0
-8.52751008119755e+02 1 0 0 0 0 1
-2.64549146780650e+01 0 2 0 0 0 0
2.48154769627209e+02 0 1 0 0 0 1
-4.97749325662935e+00 0 0 2 0 0 0

```

Bibliography

- [1] A. Adelmann et al. *The OPAL Framework Object Oriented Parallel Accelerator Library. User's Reference Manual.* http://amas.web.psi.ch/docs/opal/opal_user_guide-2.0.0.pdf. Version OPAL 2.0.0.
- [2] Martin Berz. *Modern map methods in particle beam physics*. eng. ISBN: 978-0-12-014750-2. San Diego: Academic Press, 1999.
- [3] Bernard W Stewart, Weltgesundheitsorganisation, and Centre International de Recherche sur le Cancer. *World cancer report*. eng. Lyon: IARC Press, 2014. ISBN: 978-92-832-0429-9.
- [4] Harald Paganetti. *Proton Beam Therapy*. IOP Publishing, 2012. ISBN: 978-1-4398-3645-3.
- [5] F. Hinterberger. *Physik der Teilchenbeschleuniger und Ionenoptik*. 2nd ed. Springer, 2008. ISBN: 978-3-540-75282-0.
- [6] A. Adelmann. “Lecture Slides - Particle Accelerator Physics and Modeling”. <http://amas.web.psi.ch/> & <http://amas.web.psi.ch/people/aadelmann/ETH-Accel-Lecture-1/> & <http://amas.web.psi.ch/people/aadelmann/ETH-Accel-Lecture-2/>.
- [7] Matthias Bartelmann et al. *Theoretische Physik*. deu. ISBN: 364254617X. Berlin, Heidelberg: Springer Berlin Heidelberg, 2015.
- [8] Alex J. Dragt. “Lie algebraic methods for charged particle optics”. eng. In: *AIP Conference Proceedings*. Vol. 177. 1. American Institute of Physics, Dec. 1988, pp. 261–264. ISBN: 0-88318-377-3.
- [9] Andrzej Wolski. “Alternative approach to general coupled linear optics”. eng. In: *Physical Review Special Topics. Accelerators and Beams* 9.2 (Feb. 2006). ISSN: 1098-4402. URL: <https://doaj.org/article/dfd9a560c1f4432b92f5d434f5619e18>.
- [10] Dan T. Abell, Eric McIntosh, and Frank Schmidt. “Fast symplectic map tracking for the CERN Large Hadron Collider”. eng. In: *Physical Review Special Topics. Accelerators and Beams* 6.6 (June 2003). ISSN: 1098-4402. URL: <https://doaj.org/article/08116996a6e84824a292453d4bfc52c6>.
- [11] M. Galassi, J. Davies, and J. Theiler. *GNU Scientific Library Reference Manual*. 3rd ed. ISBN: 0954612078.
- [12] K. Makino M.Berz. *COSY INFINITY 10.0. Programmer's Manual*.
- [13] A. Adelmann and M. Frey. *pyAcceLEGOrator*. SHA: 0883598fc605105fe2123264fd2a1d27ca64f7dc. 2017. URL: https://gitlab.psi.ch/frey_m/pypam1.git.
- [14] P. Ganz. “Higher dose rates for PSI Gantry 2 using new optimization tools”. Semester Project. PSI, ETH Zurich.
- [15] Richard Fenning. “Novel FFAG gantry and transport line designs for charged particle therapy”. Brunel University, 2012.